A Comparison of Grain Boundary Morphology of RRR 300 and RRR 500 Niobium After Various Polishing Processes, and Possible Implications for Q-Slope

By Jeremiah Shipman

1. Introduction

Resonant radio frequency cavities made of the superconductor niobium are used in Cornell's particle accelerator to energize the particle beams. The effectiveness of these cavities in imparting energy to the particle beam may be represented by two performance features: the accelerating electric field (E_{acc}) achieved, and the quality factor (Q) of the cavity, which characterizes how good a resonator the cavity is. Q is specifically defined as the ratio of total energy stored in the cavity to energy lost per radian in the RF cycle,

$$Q_0 = \frac{\omega U}{P_{diss}}.$$

Several factors can limit the accelerating fields which can be achieved in these superconducting radio frequency (SRF) cavities, including thermal breakdown in the niobium, field emission from contaminants on the cavity's inner surface, and exceeding the niobium's critical magnetic field (thus forcing it out of the superconducting state). The problem of thermal breakdown has been gotten around by purifying the niobium, and the field emission has been reduced by high-pressure rinsing and assembling cavities in a clean room[1]. This should leave the critical field of the superconductor (about 2000 Oe, which corresponds to about 50 MV/m accelerating electric field) as the limiting factor; yet it has been observed that cavities experience increasing RF losses (hence a decline in cavity quality) and subsequently break down somewhat sooner than this limit (at about 25 MV/m) (Figure 1).

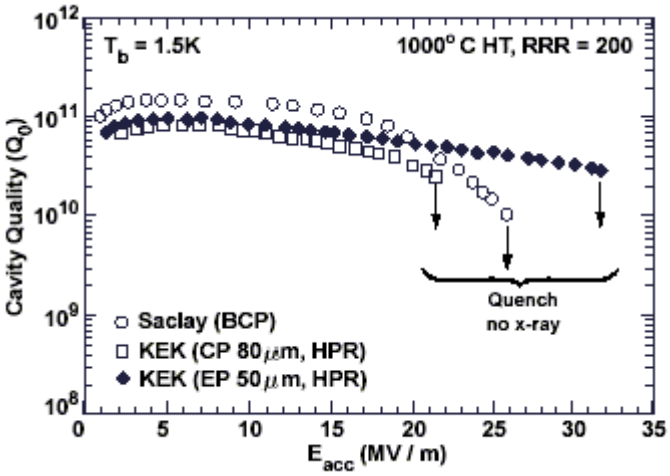

Figure 1: Q-slope is visible in the white circles (BCP etch) and is seen to diminish after electropolishing (black diamonds). From [1].

One model for the Q-slope phenomenon has to do with magnetic field enhancement on the surface of the cavity at grain boundaries. Chemical polishing (acid etching, see section [2.1.1]) is used to clean the surface of the cavity and round out machining marks. But as grains in the niobium etch at slightly different rates (due to differences in lattice orientation), the boundaries between grains are often marked by microscopic steps. These sharp steps locally enhance the magnetic field to values higher than the critical value needed to change the niobium back into a normal conductor. As this happens on a small scale and as there is a distribution of field enhancement factors (coming from a distribution of geometries at grain boundaries), this results in a slow decline in cavity quality (Q-slope) followed by a somewhat early breakdown[1]. This problem can be ameliorated by better smoothing the surface of the cavity, through techniques other than the standard buffered chemical polish (BCP, section

[1]J Knobloch et al, High-Field Q Slope in Superconducting Cavities Due to Magnetic Field Enhancement at Grain Boundaries, *Proc. of the 9th Workshop on RF Superconductivity*, Santa Fe, NM (1999).

2.1.1). Electrolytic polishing (EP, section 2.1.2) been shown to smooth the surface quite nicely, eliminating the Q-slope and allowing accelerating fields of up to 40 MV/m before breakdown[1]. This study explores the effectiveness of a few other polishing techniques on two different purity grades of niobium (RRR 300 and 500, section 2.1.5), and compares the geometry of the grain boundary features using a scanning electron microscope (SEM, section 2.2.1), a surface profiler (section 2.2.2), and an atomic force microscope (AFM, section 2.2.3).

2. Methods and Tools

2.1. Polishing Methods

2.1.1. *Chemical polishing.* I tried several chemical polishing recipes: BCP 1:1:2 (49% concentration hydrofluoric, 69.6% nitric, and 86.0% phosphoric acids in the ratio 1:1:2), BCP 1:1:1, FNS 1:1:1 (hydrofluoric, nitric, and 96.4% sulfuric acids in the ratio 1:1:1), and FNS 1:1:2. The BCP is our standard recipe, and the FNS was suggested in a paper[2]. Additionally, I oxypolished and examined two samples, and also had the opportunity to examine an electropolished sample and several samples polished by gas-cluster ion bombardment (GCIB).

Cavities will typically receive at least 100 microns (μm) of etching in a mixture of acids known as buffered chemical polish, or BCP, 1:1:2 -- a mixture of hydrofluoric acid (HF), nitric acid (HNO_3), and phosphoric acid (H_3PO_4) in the ratio 1:1:2 and at less than 15°C – as part of their treatment. The nitric acid oxidizes the niobium, the hydrofluoric reduces the niobium oxide to a soluble salt,

[2] Antoine CZ et al, Morphological and Chemical Studies of Nb Samples After Various Surface Treatment, Proceedings of the Ninth Workshop on RF Superconductivity, November 1-4, 1999, Santa Fe NM LA-13782-C, p.295

and the phosphoric moderates the reaction and makes it more controllable[3]. The etch rate varies with temperature and composition (ratios other than 1:1:2 are occasionally tried), but is typically about 2 μm/min at 25°C [my measurement].

Rather than using entire cavities, for my surface studies I used small (surface areas of a few cm^2) niobium samples that were easier to handle. I would typically mix up a chemical polish that I was interested in trying and let it settle or cool for a few hours (some of the mixtures would heat up considerably upon the initial mixing) during which time I would preclean my sample in soapy water with a soft cloth and then ultrasonically in methanol, and dry it. I would then etch my samples in a small cup of the acid under a fume hood and with proper protective equipment. To achieve removal of 100μm, I would soak the sample in the acid for 20-50 minutes, stirring occasionally with a Teflon-coated thermometer or with a Teflon-coated magnetic stir bar. I would then remove the sample from the acid and rinse it with ultra-pure deionized water for up to 10 minutes (to make sure the acid was removed) and hang it to dry under a clean hood in a clean room. In the case of some treatments which were particularly reactive (eg, hydrofluoric-nitric-sulfuric (FNS) mixtures), I refrigerated the mixture before etching in order to better control the etch.

I also measured etch rates for some of the new recipes: For BCP 1:1:1 etching from at temperatures in the range 23°C to 27°C, I measured a mean etch rate of 2.7 (+/- 0.4) μm/min. For FNS 1:1:1 with a starting temperature of -10°C and a

[3] V Palmeri et al, Besides the Standard Niobium Bath Chemical Polishing, The 10th Workshop on RF superconductivity, 2001, Tsubuka, Japan

final temperature of 10°C, I measured an etch rate of 5.6 (+/- 0.6) μm/min. For FNS 1:1:2 with temperatures ranging in the range of -8°C to 3°C, I measured an etch rate of 4 (+/-1) μm/min. Etches were typically 20-30minutes long, for totals of 75-100 microns of material removed.

2.1.2. *Electropolishing.* In this technique, the niobium is made the anode in a chemical bath which is a conductive mixture of hydrofluoric and sulfuric acids[4]. The electric field provides the oxidizing force, so nitric acid is not needed as it is in BCP. As the electric field in the solution is geometrically enhanced at pointy features, any sharp peaks in the niobium are preferentially etched[5]. Hence, electropolishing smoothes the surface. I did not perform this process, as there was a sample available for me to examine which had already undergone the treatment.

2.1.3. *Oxypolishing.* Oxypolishing is a technique in which the niobium is alternately subjected to anodic oxide growth and etching in hydrofluoric acid as a means of surface removal. The hope was that the anodic oxide growth would preferentially target pointy (field-enhancing) spots on the surface of the niobium for oxidation, thus when the oxide was removed by an HF bath, the surface would be smoother.

[4] K Saito, Development of Electropolishing Technology for Superconducting Cavities, Proceedings of the 2003 Particle Accelerator Conference, May 12-16, 2003, p. 462

[5] Improved Surface Treatment of the Superconducting TESLA Cavities, L. Lilje et al, Nucl.Instrum.Meth. A516 (2004) 213-227, DESY 2004-17, TESLA 2004-04

In order to anodize the samples, a bath of 0.015% ammonium hydroxide (NH_4OH) solution was prepared (stronger solutions would normally be employed, but as my samples were so small, I opted for a weaker (and thus safer and easier to handle) solution). A niobium cathode was partially submerged in the bath, as was the anode: the sample to be anodized, which was either strung up on a niobium wire (one sample had a bolthole in it) or held with "tongs" fashioned from niobium wire. (it is important that all of the submerged electrodes be niobium, so that no other oxides form and contaminate the solution or the sample.) A Niobium oxide (Nb_2O_5) is known[6] to form anodically to a thickness of about 20 Angstroms / volt. This setup is shown in Figure 2. The voltage difference between the electrodes was then increased to the desired voltage (typically 60-100 V), recording the current density. For the two different samples, I did this differently (though the results were essentially the same). For the first sample, I simply turned on a voltage as high as 60 V and waited for the current to drop to about 1% of its initial value. This generally took about 5 minutes [see appendix 1 for current measurements]. Then, if I desired a higher voltage, I would turn the supply up quickly and wait again for the current to drop. Current densities for this run were typically about 4 mA / cm^2, though there were briefly peaks of up to 20 mA/cm^2 when the voltage was first applied. For the second sample, I was concerned that this rapid growth may have lead to an uneven or irreproducible oxide layer, so I turned the voltages up much more slowly. In this case, the current density never peaked over 2 mA / cm^2 but the anodization took up to 45 minutes to complete. It may be worthy of note that the highest voltage that I ever

[6] Halama H J 1971 *Particle Accelerators*, vol 2 (New York: Gordon and Breach) pp335-341

used was 120V, and the linear 20A/V relationship is known to work up to about 180V[7]. Once the oxide was grown, the sample was removed from the ammonium hydroxide solution, rinsed with ultra clean water, and moved to a different fume hood[8] where it was immersed in 49% HF for about 5 minutes. This removed the oxide layer completely, and the cycle was started again.

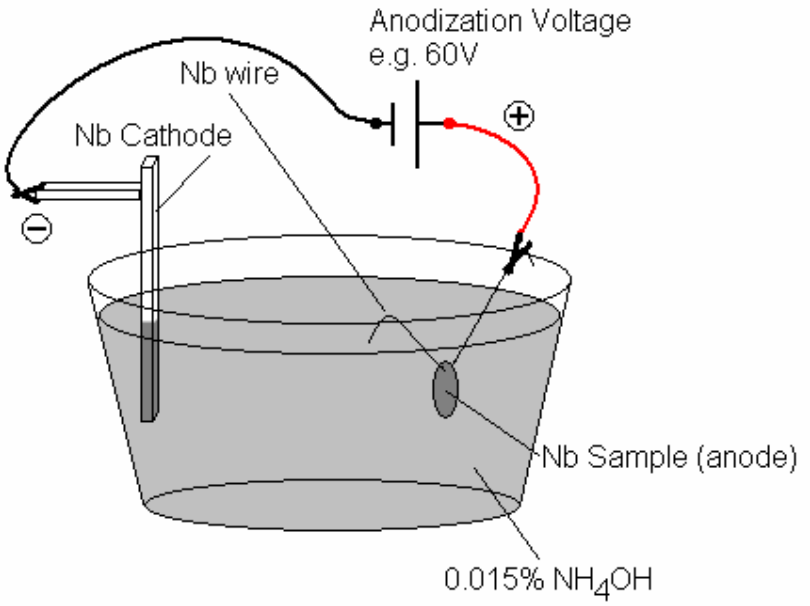

Figure 2: Anodization setup

Since each cycle would grow and remove an oxide layer of a thickness of order 1000 Angstroms, many cycles would be required to etch an appreciable amount off the sample. Because I found the roughness of my samples to be of order a few microns, and because oxypolishing is somewhat slow going, I aimed to etch approximately a micron over the course of 4-6 cycles in my process in order to see any effect.

---

[7] K C Kalra, K C Singh, M Singh, Formation and Breakdown Characteristics of Anodic Oxide Films on Valve Metal, Indian Journal of Chemistry, Vol 36A, Mar 1997, pp.216-218

[8] I was told that HF and NH_4OH should not be used in the same fume hood, as their vapors may react in a dangerous way.

2.1.4. *Gas Cluster Ion Bombardment (GCIB).* GCIB is a polishing technique in which clusters of gas molecules are partially ionized, then accelerated and directed into the target material. These clusters thus have a high total energy, but a low energy per particle. In comparison to bombarding the target with single ions which can penetrate the surface and deposit their energy deep (>1000A) into the material, these clusters cannot penetrate very deeply into the substance (<100A) and thus deposit all of their energy in a localized region right on the surface (Figure 3)[9].

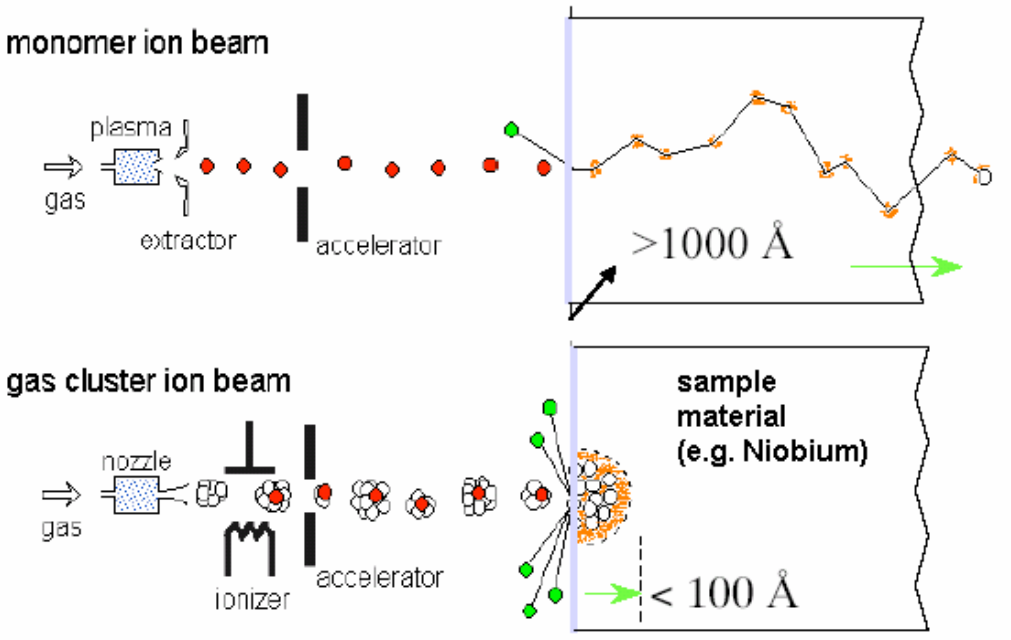

Figure 3: GCIB explanatory diagram, from [9]

[9] Z Insepov et al, "Field Evaporation and GCIB Processing of Electrodes," Workshop on High Gradient RF, at Argonne Nat'l Laboratory, Oct 7-9, 2003

Colleagues[10] were kind enough to perform GCIB polishing with several different gasses on some niobium samples for us, and the results of the processes are examined.

2.1.5 *Higher Purity Niobium.* In addition to these polishing techniques, some investigations were made into the effect of using a higher purity niobium as the test sample. Most of the samples used were Residual Resistivity Ratio (RRR) 300 niobium. However, some measurements were made with higher purity RRR 500 niobium. The RRR is usually defined as the ratio of the resistivity of the material at room temperature to that at liquid helium temperature. That is,

$$RRR \equiv \frac{\rho_{300K}}{\rho_{4.2K}}$$

However, since niobium is a superconductor at liquid helium temperature, the value used is actually the normal-conducting resistivity extrapolated down to 4.2 K or obtained by quenching the SC state with a magnetic field. A material with more impurities and lattice defects has a lower RRR. Hence RRR makes a fair measurement of the purity of the niobium: the higher this number, the more pure the niobium.

2.2. Surface Characterization Tools

2.2.1. *Scanning electron microscope.* For a general, quality image of the surface of the samples, I used a scanning electron microscope (SEM). The microscope is a good general purpose tool, because it has a large depth-of-focus

[10] Thank you to David Swanson and others at EPION Corp. for offering to do this polishing.

and it can be used to take large scale pictures of areas in addition to taking small scale images with resolutions of about 100 nm. I used the microscope to get a good idea of what the surface looks like and sometimes to make “maps” of a sample to help navigate on other instruments (like the AFM) and find interesting features. The microscope works by focusing a beam of energetic (20 keV in my case, though this may be changed) electrons into a spot on the surface, and then collecting any secondary electrons which are emitted from the surface as a result of the impact. The spot is then rasterred over the surface of the sample. In this way, information about the secondary-emission properties of the surface are collected with a resolution of about the spot size. Because the electron detector is located on one side of the SEM chamber (Figure 4), and because the sample may be tilted, it is also possible to collect information about the surface morphology (surfaces which are oriented away from the detector will appear dimmer, since fewer of their secondary electrons will make it to the detector).

Figure 4: Scanning electron microscope. Above: the instrument. Below: inside the chamber with the door open. Note that the secondary electron detector is off to the side, rather than directly above (the primary electrons come from directly above).

2.2.2 *Surface profiler.* To collect quantities of information about the roughness of the surfaces of samples, a surface profiler was used. This device (Figure 5) consists of a small needle, which is dragged over the surface of the sample (in one-dimension only), while its vertical motion is recorded. The tip of

the needle is a cone with a 60-degree slope, and the point has a radius of curvature of about 5 microns (Figure 6).

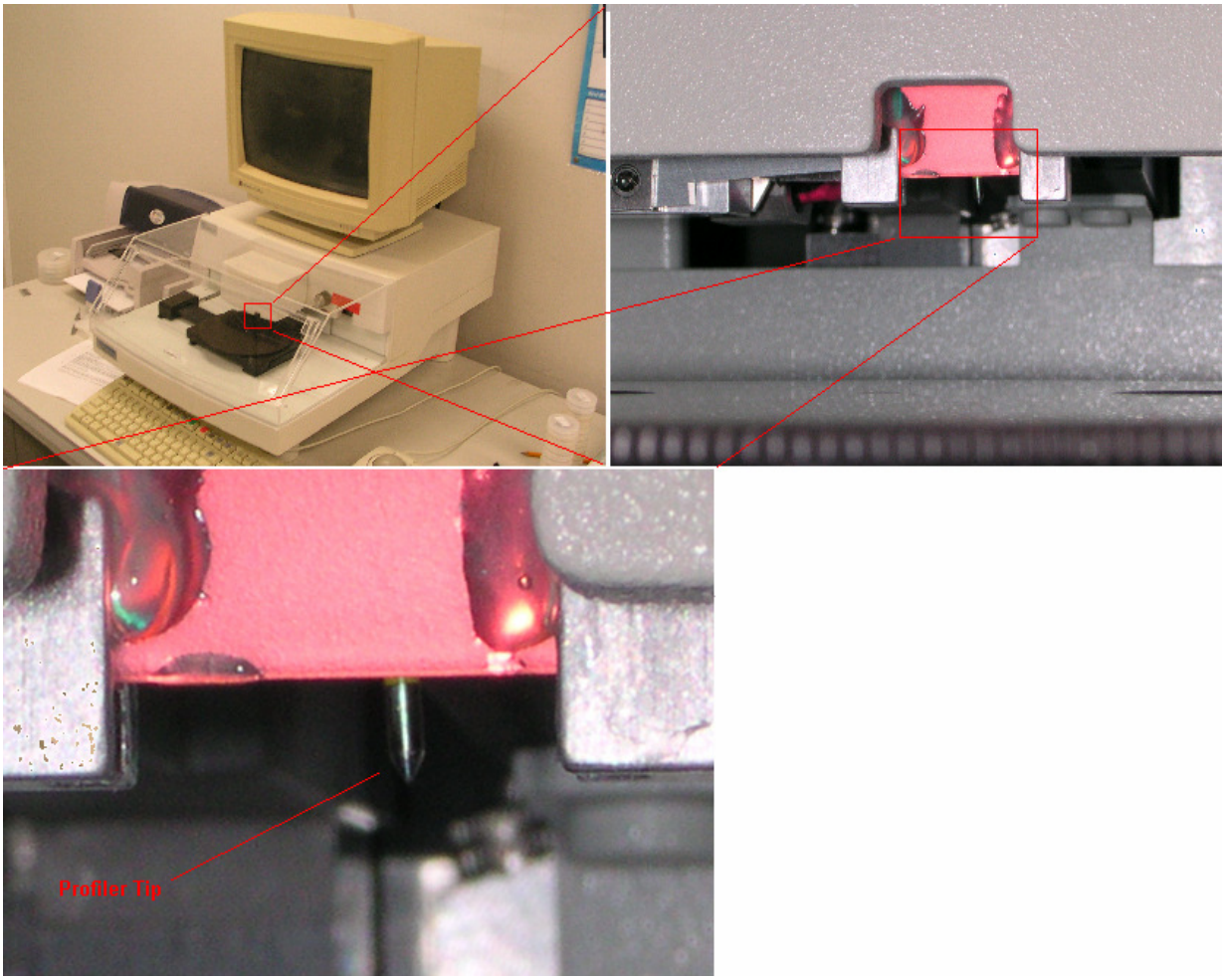

Figure 5: Surface profiler and tip closeup

The shape of the tip will, of course, limit the information that may be gained about small-scale structure in the sample. However, as the grains in the niobium I was studying were on a size scale of about 50 μm, the tool was useful for looking at grosser aspects of grain structure, and for generally comparing the smoothness of the samples at that scale. Also, the tool is very quick to use and so it is

possible to collect large amounts of data over large sample areas, which may be statistically meaningful.

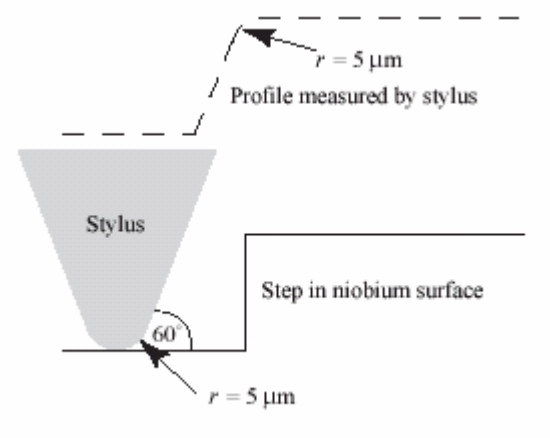

Figure 6: Surface profiler tip shape, from [1]

2.2.3. *Atomic force microscope.* For precise examinations of the shape of grain boundaries or other features at the very small scale, an atomic force microscope (AFM) (Figure 7, left) was used. Like the surface profiler, the relevant part of the AFM is the tip, which is conical and is used to probe the surface features by physically touching the sample (though the AFM as I used it would tap the tip into the surface at some sampling rate, rather than dragging the tip along). However, there are several important differences. Primarily, the tips (Figure 7, right) are much smaller and pointier—the design I used have a radius of curvature of a few tens of nm and have a slope angle of about 40° (they are micromanufactured and disposable, so that a new one may be used for each sample, to assure one that the tip, which is very fragile, has not been damaged). Secondly, the tip is rasterred over the surface to create a three-dimensional surface image. This is a somewhat slow process, and the instrument is

occasionally tricky to use due to its small dynamic vertical range (about 6 microns), so it is hard to collect large amounts of data with the AFM. However, it is possible to get very good images of very small features.

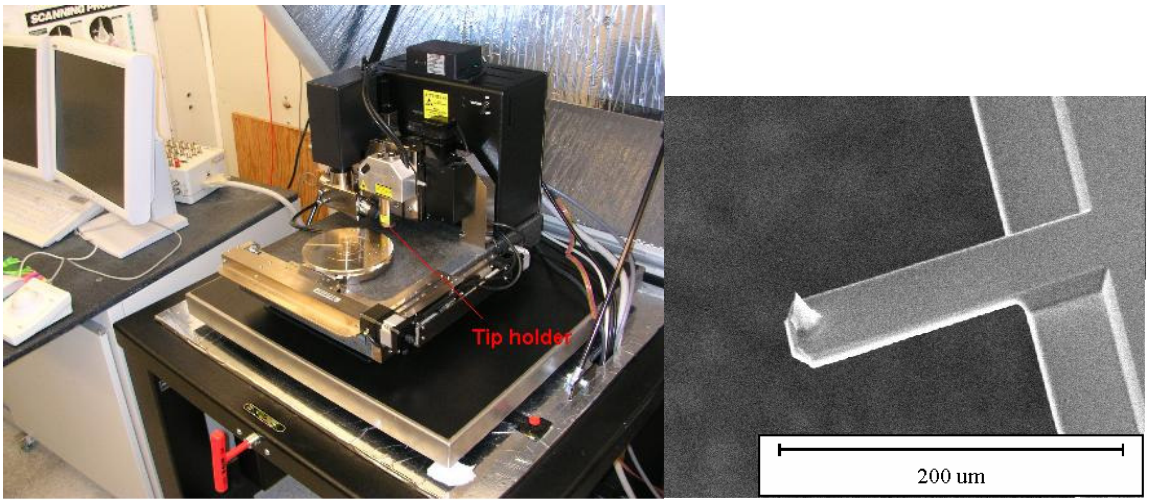

Figure 7: Atomic force microscope, and SEM image of an AFM tip.

2.3. Data Analysis and Visualization Methods

2.3.1. *3D SEM*. Because one can tilt the sample in the SEM, It is possible to produce 3-dimensional (stereoscopic or anaglyph) images with the instrument. It would be hard to use these images for quantitative measurements of grain boundary morphology, but it is useful for visualization purposes, to better develop an intuition for what the grain boundaries look like. The idea is an old one[11], but is made easier with digital photo manipulation. The basic procedure is to take a head-on image with the sample untilted. Then, tilt the sample 8 or so degrees, and take another picture of the same feature. Then using an image manipulation tool such as photoshop or the GIMP (Gnu Image Manipulation Program) you can

[11] L. Marton, Stereoscopy with the Electron Microscope, J. Appl. Phys. **15** (10) pp.726-7 (1944)

overlay the two images on different layers and remove the red from one, and the blue and green from the other. You now have a composite image of the same feature offset to eyes looking at it through cellophane red-blue 3D glasses (Figure 8). More detailed instructions may be found in appendix 2.

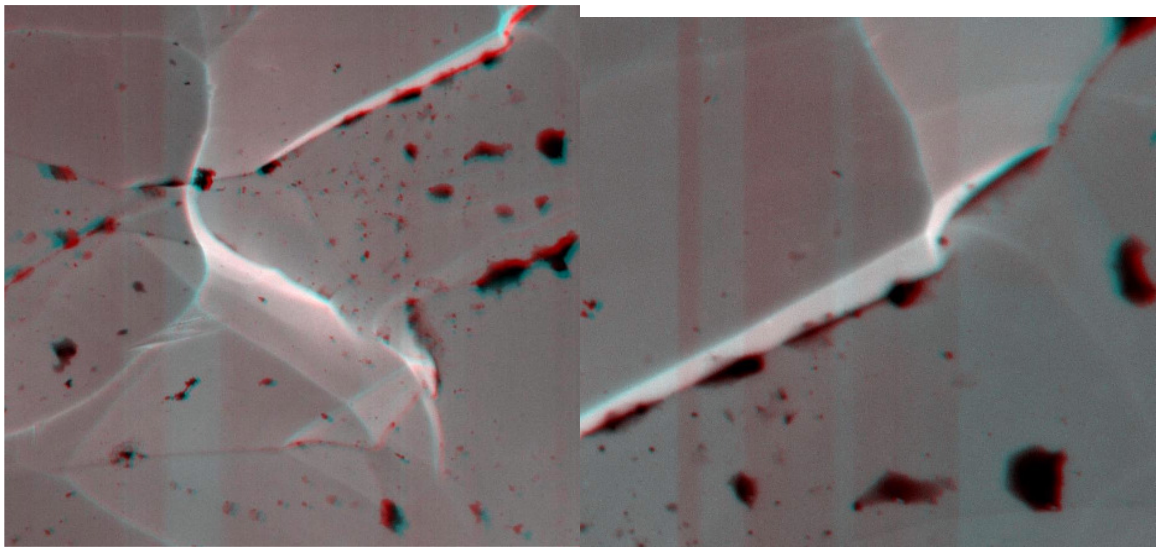

Figure 8: 3D SEM images. The black spots are the result of placing the sample in a nylon bag for storage, and are not relevant to the discussion. (The nylon may be removed with a light etch).

2.3.2. *Collecting profiler data.* As it is not possible to determine exactly where on the sample the profiler tip is, say, for comparison with SEM images, it is necessary to take rather a lot of data with the profiler and try to learn things on a statistical basis. The profiler software allows data to be exported in ASCII format, as pairs of numbers (microns in the horizontal dimension, and microns or nanometers in the vertical dimension—a height profile). I recorded surface profiles, typically of a length of 2000μm, at 10 or so random locations on each sample. I then used MATLAB to subtract out any linear slope (to try to compensate for the sample not being quite flat on the table) and then look at the deviation from the level (a typical profile, Figure 9). I extracted the standard

deviation from the level, and also looked at the distribution of heights—how much time one would spend at each height, if one were walking along the surface of the sample. I considered trying to measure angles and radii of curvature of grain boundaries, but the clumsy size of the stylus would have limited the usefulness of this.

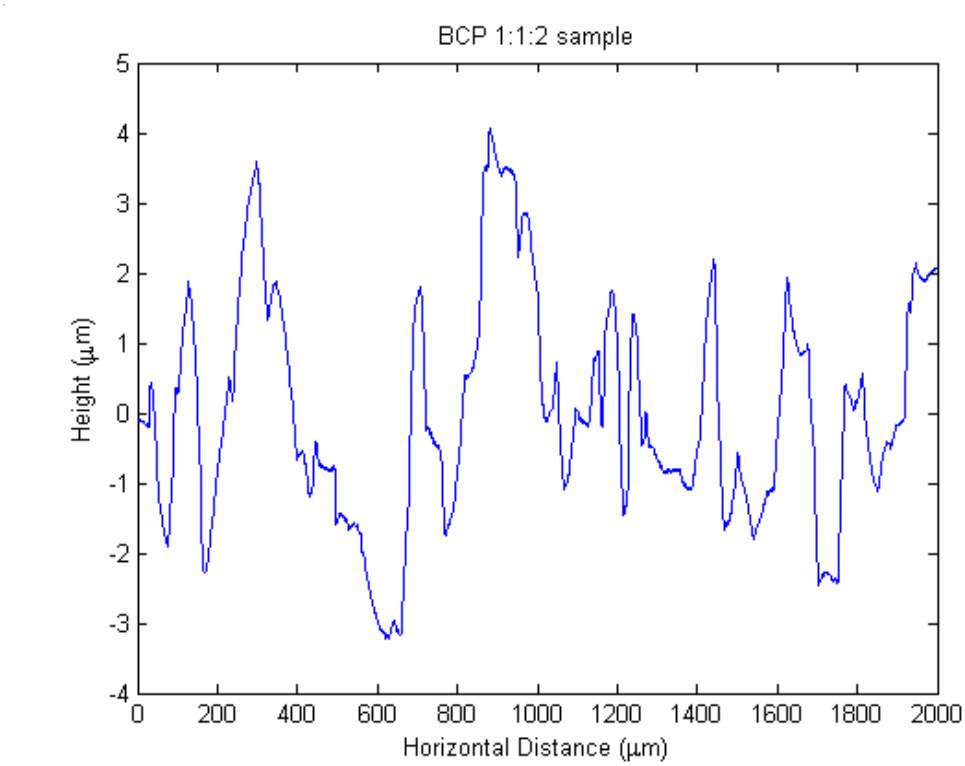

Figure 9: A profile taken from an RRR300 BCP 1:1:2 sample. Note the different horizontal and vertical scales.

2.3.2. *Extracting details of grain boundary morphology from AFM measurements.* As mentioned before, the AFM gives a high resolution, 3-dimensional image of a surface. It was used to take images of many grain boundaries, which had undergone different surface treatments. These surface images were again exported in an ASCII format. To extract useful information about the precise shape of the grain boundaries, I read the ASCII data into

MATLAB, where I wrote a small function to plot the surface and allow me to take an arbitrary cross section in the image (Figure 10), and to fit a pair of lines and a portion of a circle to that cross section. When viewing these images, please note the difference in scale on the vertial and horizontal axes. The vertical axis is almost always stretched, giving the features a very exaggerated look and possibly making the labeled angles seem incorrect. This allowed me to measure the angle and radius of curvature which characterize the sharpness of the grain boundary. Objects with sharper peaks and smaller radii of curvature have higher magnetic field enhancement factors, and I believe that these are the measurements relevant to calculating (or at least estimating) the grain boundary's magnetic field enhancement factor. In some of my pictures, the resolution was insufficient to fit a radius of curvature. In these cases, I estimate (as an upper bound) the radius to be twice the spatial resolution (ie, twice the mesh size).

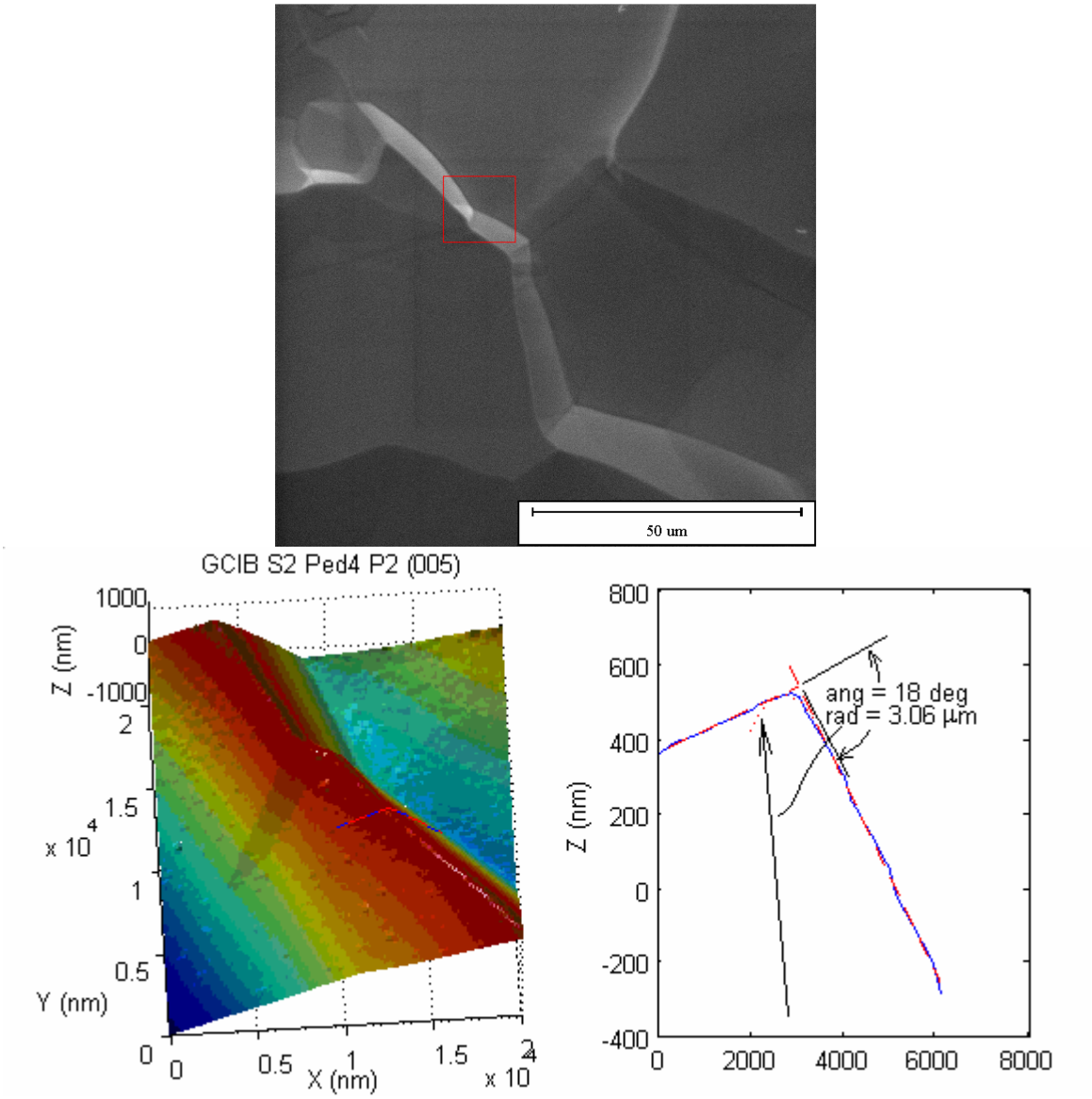

Figure 10: SEM image of a grain boundary (top). AFM image of same grain boundary, cross section with labeled angle and radius of curvature (bottom). The circle looks odd due to the difference in horizontal and vertical scales—but it is a portion of a circle.

3. Results and Discussion

3.1. Profiler. As mentioned above, the profiler does not give fine-shape information. However, it does give a very good measurement of the large-scale ups-and-downs present in the surface and can be suggestive of overall

roughness or smoothness. The shapes of the height distributions can also be revealing.

3.1.1. *RRR 300 BCP 1:1:2.* As a baseline, consider this RRR 300 BCP 1:1:2 measurement (Figure 11). Notice how the horizontal scale of the roughness (corresponding to the grain size) is in the 50-100μm range. Also notice how the distribution's (Figure 12) peak is shifted somewhat toward the "more rough" side of center (for the purposes of making these histograms, I defined zero height as the lowest point that the surface ever reached, so that the mean height is somewhere other than zero. Also, the distributions are compiled from several (5-10) profiler measurements at random areas of the sample, not just the one shown). The RMS height is written for general comparison purposes.

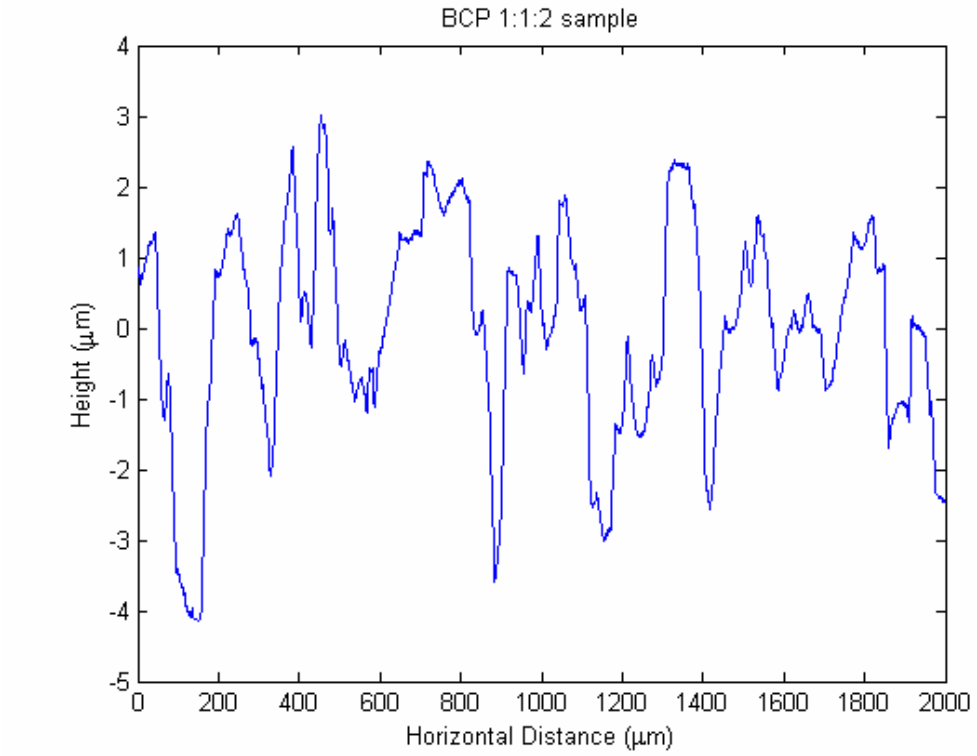

Figure 11: Surface profile of RRR 300 BCP 1:1:2

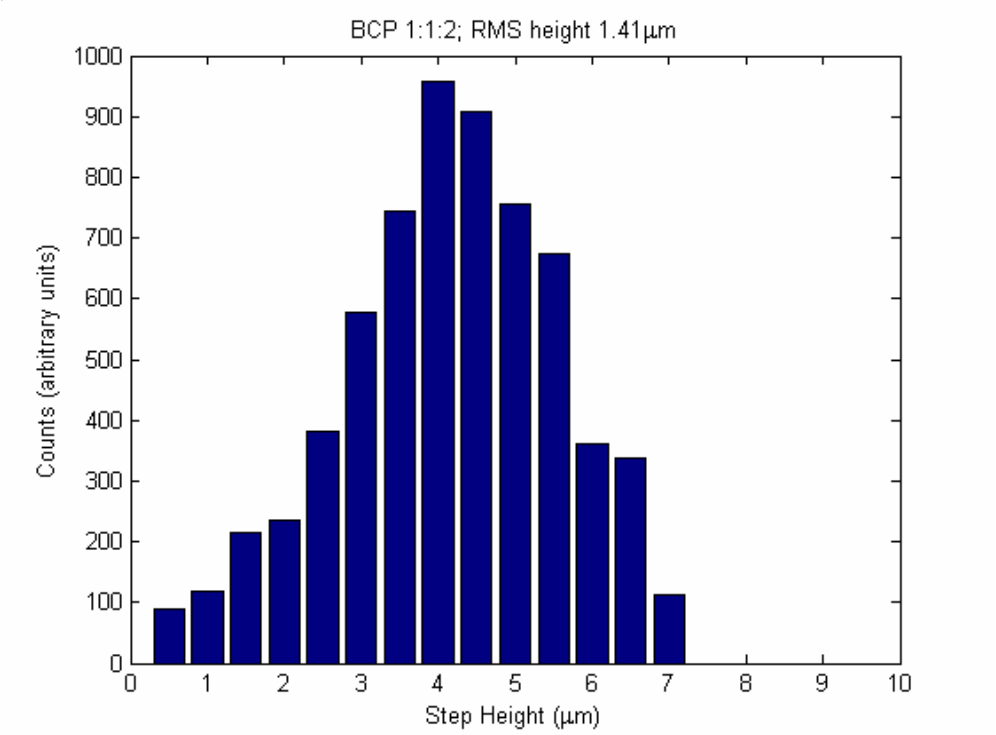

Figure 12: Histogram of heights in RRR 300 BCP 1:1:2

3.1.2. *RRR 500 BCP 1:1:2.* I also made similar measurements on a RRR 500 niobium sample which had been etched in BCP 1:1:2. The horizontal scale of roughness (grain size) seems like it might be slightly smaller (Figure 13), but it is hard to tell (a composite picture for comparison, Figure 15). Also, the distribution of step heights (Figure 14) seems somewhat smoother for the RRR 500 sample, but I am not sure what this indicates.

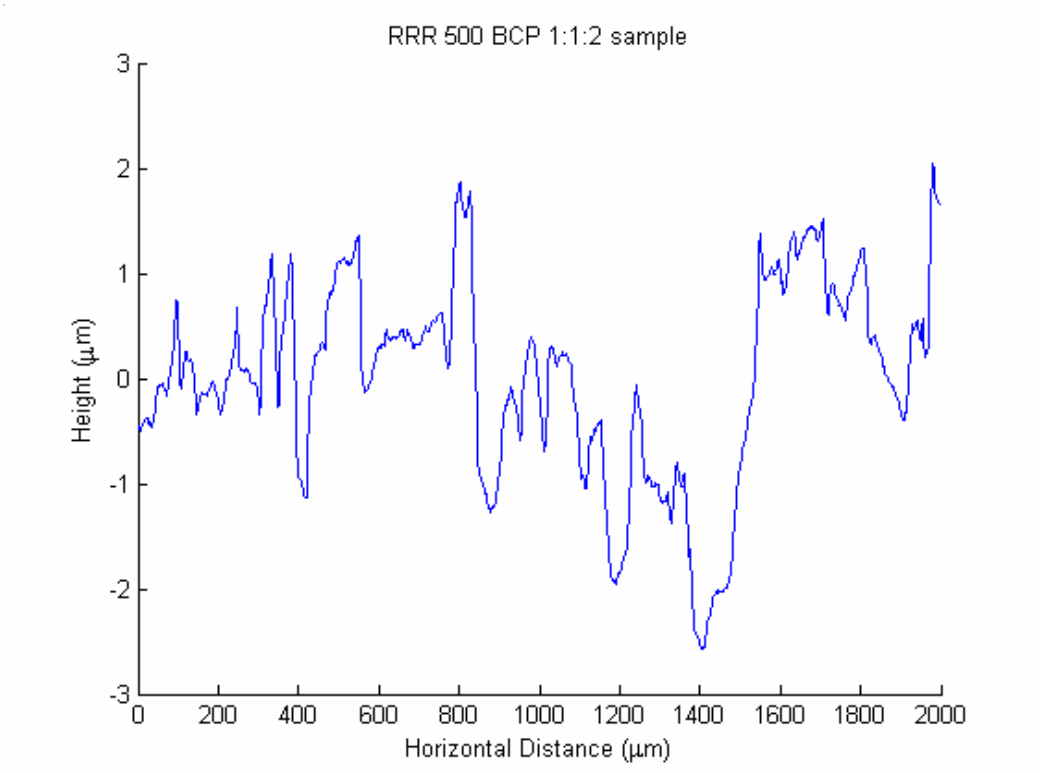

Figure 13: Surface profile of high purity niobium after etching in BCP 1:1:2

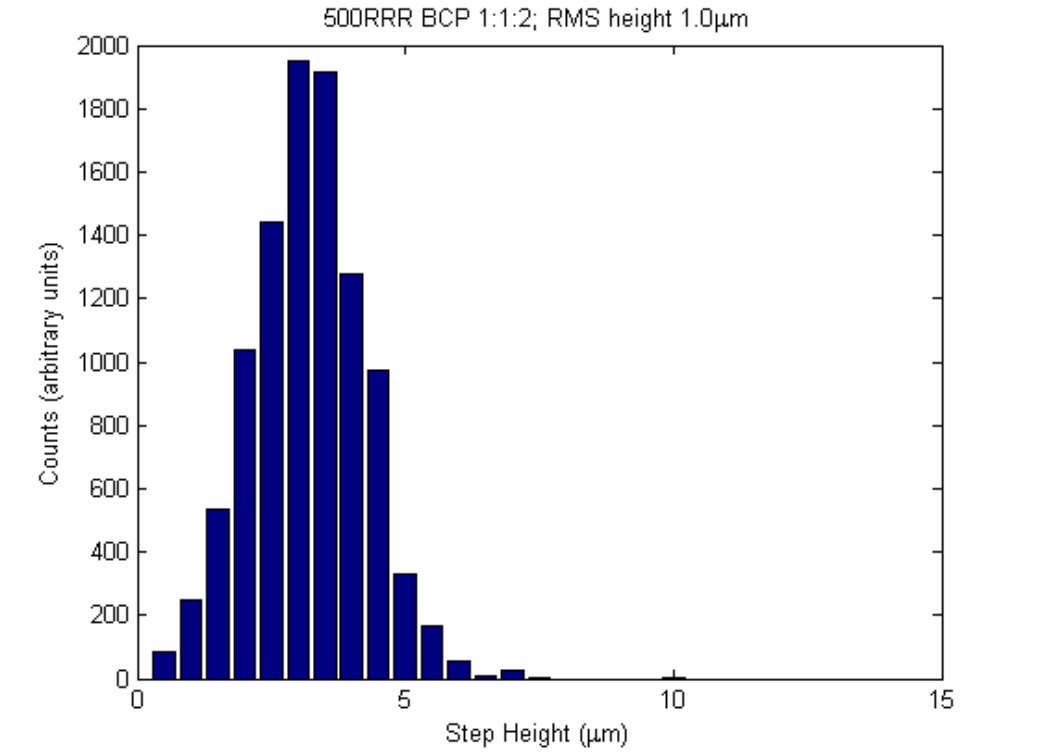

Figure 14: Histogram of step heights for RRR 500 niobium etched in BCP 1:1:2

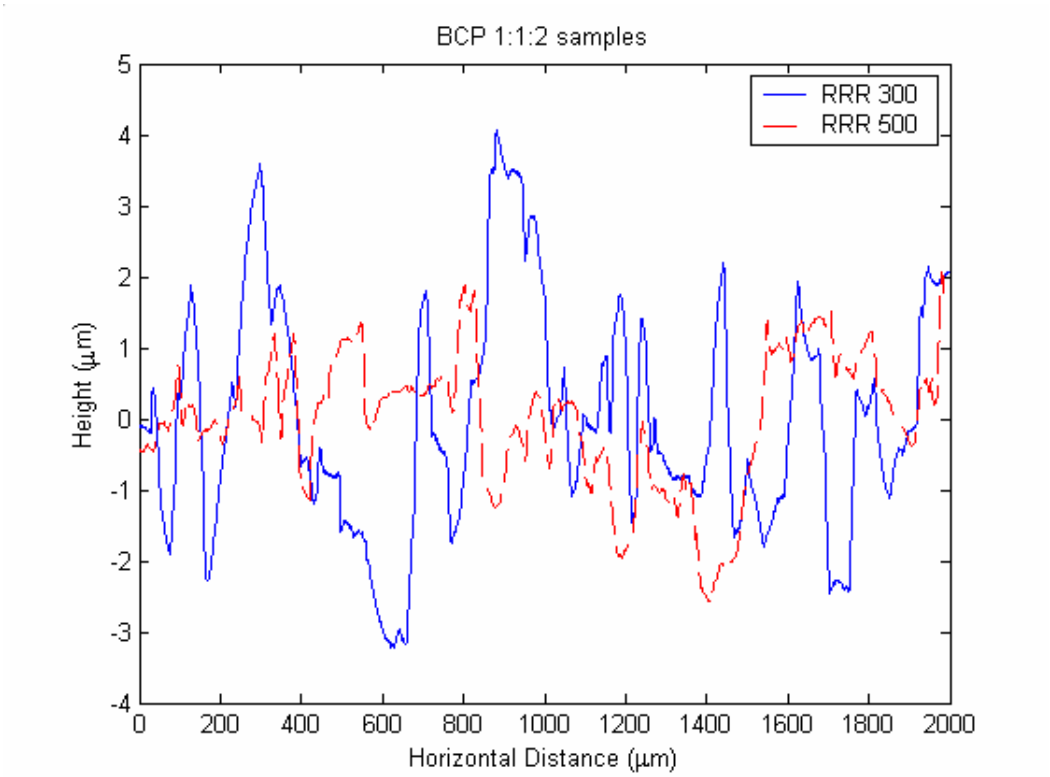

Figure 15: Comparison of profiles of RRR 300 and 500 niobium after both have been etched in BCP 1:1:2

3.1.3. *Electropolishing.* Now see the results for the electropolished sample (Figure 16, Figure 17). Again, the grain size is roughly in the 50-100μm range, but note the difference in vertical scale. The vertical resolution of the surface profiler is stated at 13 Angstroms, so the roughness we are measuring is still about a factor of 100 above that limit (but you can see how the profile is a bit noisier than that of the BCP sample). Note also the smoother shape of the distribution.

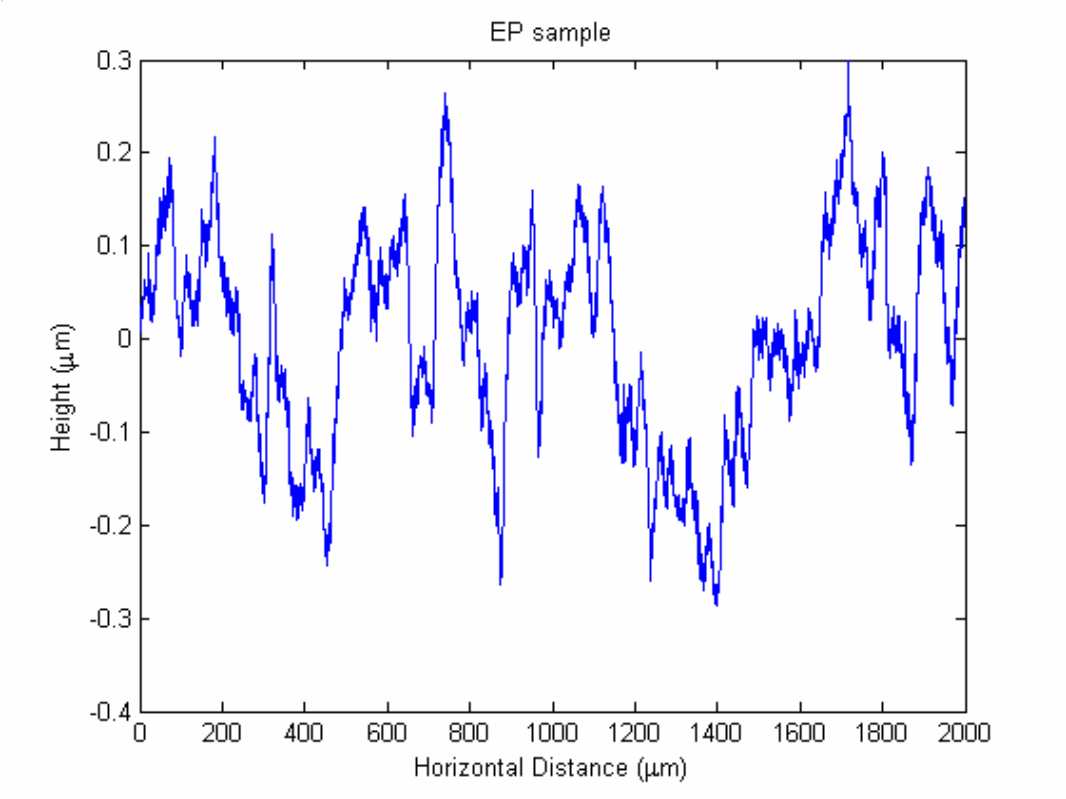

Figure 16: Electropolished sample surface profile

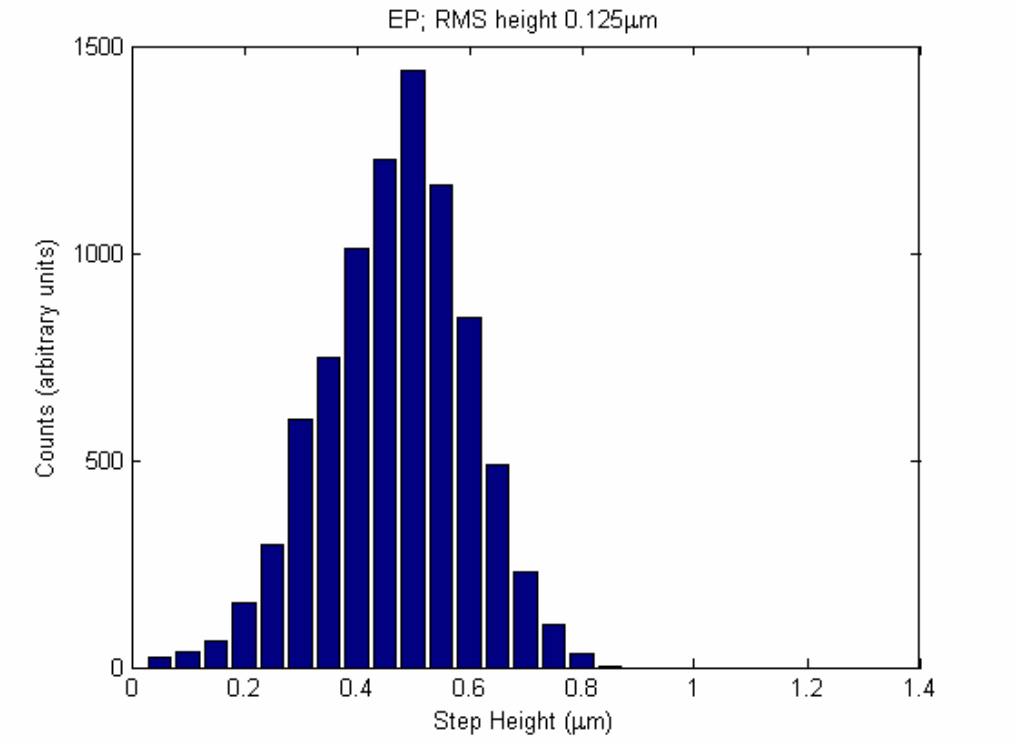

Figure 17: Electropolished sample profiler histogram

3.1.4. *RRR 300 FNS 1:1:1.* Below are results for a hydrofluoric-nitric-sulfuric (FNS 1:1:1) sample (Figure 18, Figure 19). Note first how the horizontal scale of the roughness seems to be larger than the grain size (which was the same as the other samples). This is reflected to some extent in the distribution—how it is not very smooth. An interesting point is that the profile suggests that on the small scale, the FNS may be smoother than the BCP surface, while being rougher on a large scale. This same observation was made by Antoine, et al[2]. I believe that the non-normal shape of the histogram has to do with the large-scale roughness being more comparable to the size scale on which I was taking measurements, meaning that a relatively smaller sample was taken of the large scale roughness, so poorer statistics were achieved (ie, if I took 10 mm worth of profiles, this is 200 (a good sample size) 50μm grains, but only 20 (leading to lots of statistical noise) 500μm larger features).

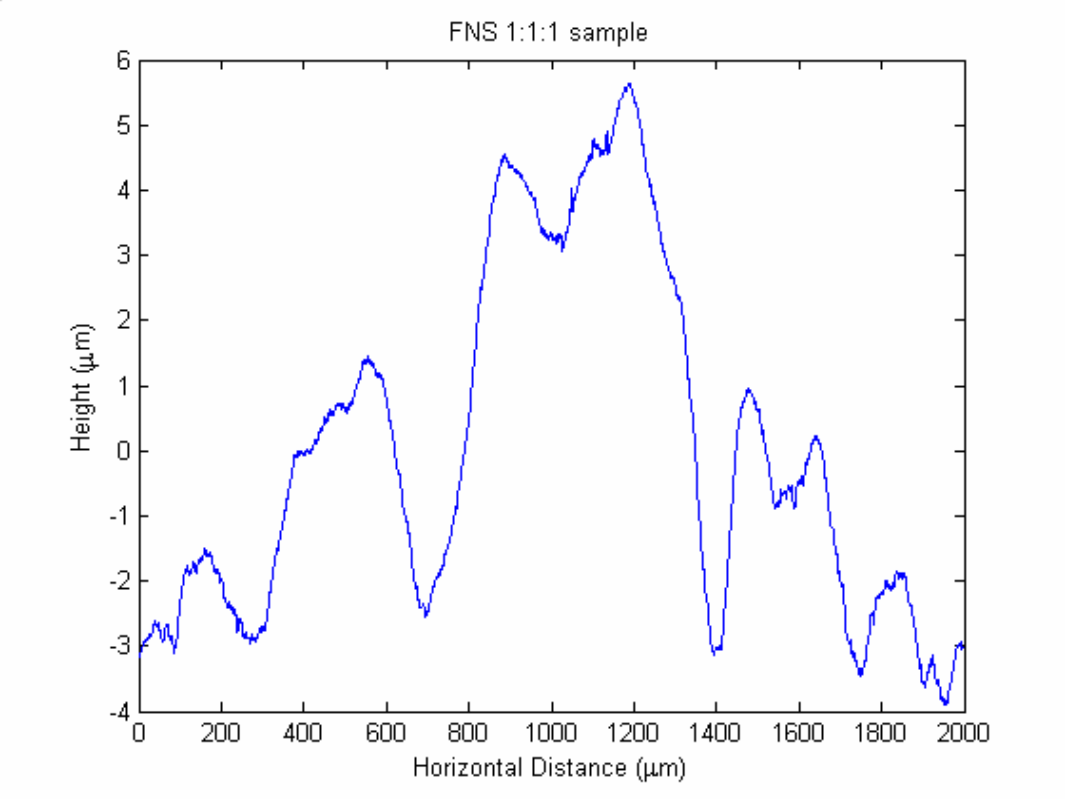

Figure 18: Surface profile for FNS 1:1:1

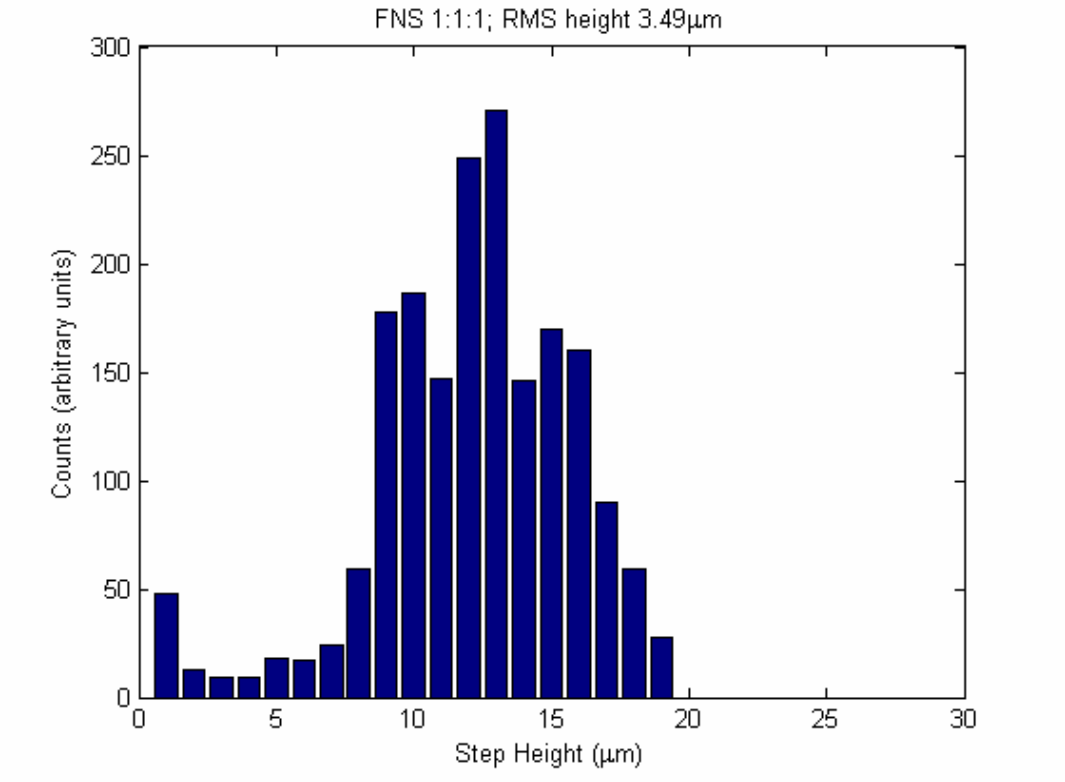

Figure 19: Histogram of heights for FNS 1:1:1

Another point of note is that higher purity niobium samples (500 RRR, as opposed to our standard 300 RRR) seemed slightly smoother.

3.1.5. *Summary*. By way of summary I will present a composite of various profiles laid out to scale (Figure 20), and a chart (Table 1) with RMS values of height. The details of the results can be found in appendix 3.

Table 1: Profiler summary

Sample	RMS Rough. (μm)	Peak-Peak Rough. (μm)	Total length profiled (μm)
BCP 1:1:2	1.41	6.26	6,500
BCP 1:1:1	1.07	4.84	8,500
FNS 1:1:1	3.49	11.7	7,500
EP	0.12	0.66	8,500
500 RRR FNS 1:1:1	2.45	11.2	10,000
500 RRR BCP 1:1:2	1.03	5.57	20,000
500 RRR FNS 1:1:2	4.61	22.8	9,000

The main result that this comparison brings out is the difference between electropolishing (the broken black line in Figure 20) and other techniques, and the difference in roughness scale between FNS (yellow and blue lines) and BCP.

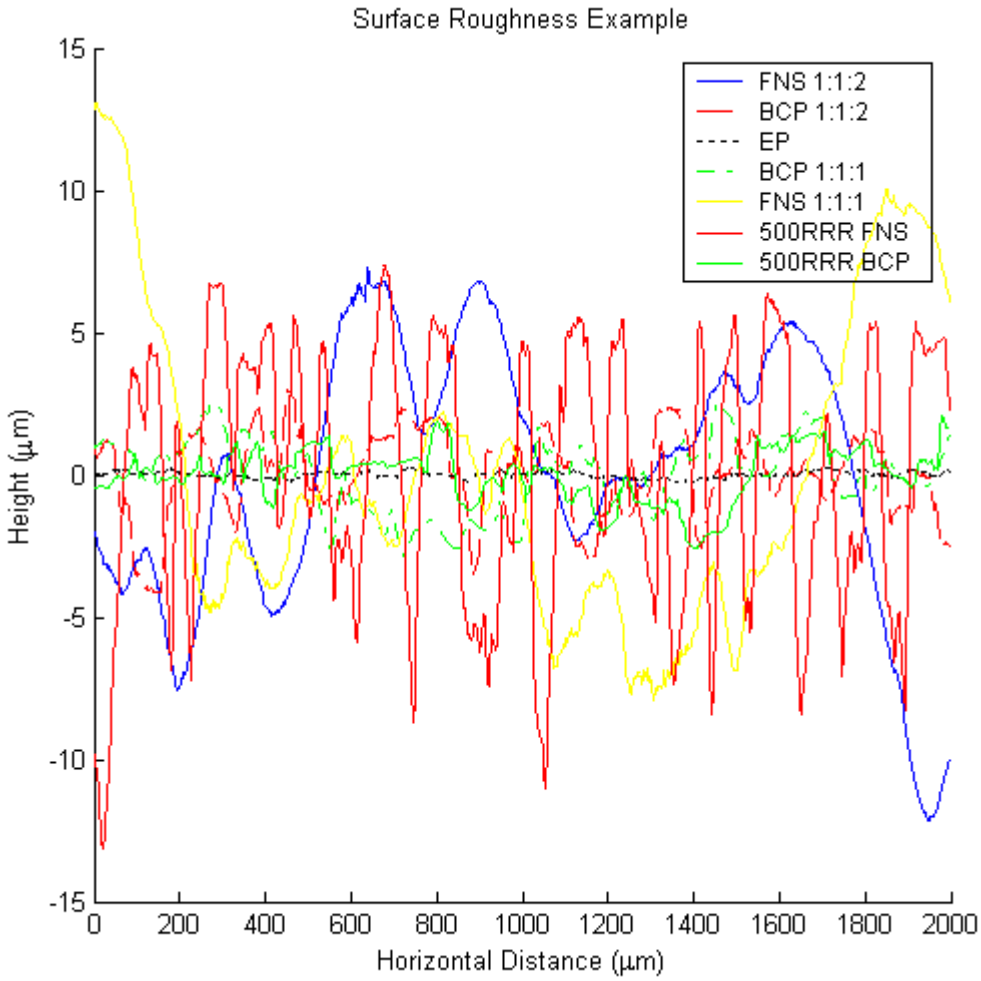

Figure 20: Comparison of profiles

3.2. AFM. As mentioned above, the AFM was used to measure the precise shape of grain boundaries, specifically the angle at which the two edges come together, and the radius of curvature of the vertex. The greater the angle and the smaller the radius of curvature, the pointier the feature, and the greater the magnetic field enhancement. My general procedure for this section was to take these measurements on 10 or so grain boundaries in each sample, in the hopes of getting an estimate of their range and compare these ranges for different

samples to see if some treatments resulted in smoother surfaces than others. In the following sections I have displayed some (but not all) of my images, which I believe to be representative of the surfaces examined.

3.2.1. *RRR 300 BCP112*: My baseline sample is 300 RRR niobium with about 95µm removed by etching in BCP 1:1:2 (Figure 21 is an SEM image of this sample, and Figure 22 is an example of an AFM image).

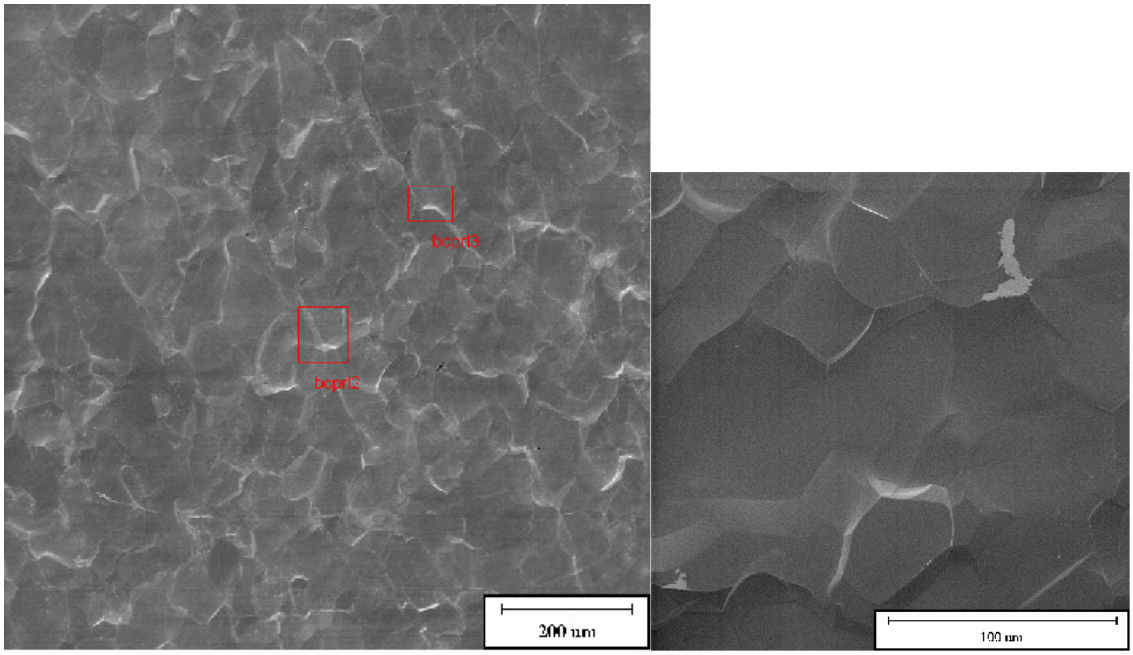

Figure 21: SEM image of RRR 300 BCP 1:1:2 samples. The scale bar on the left image is 200µm, and that on the (zoomed) right image is 100µm. Grains of ~50µm size can be seen.

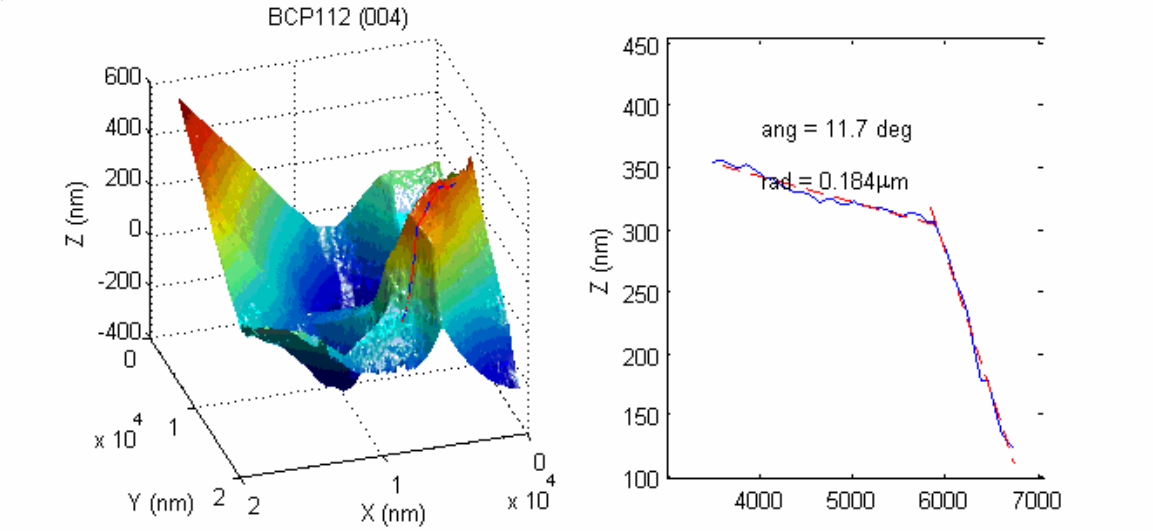

Figure 22: BCP 1:1:2 grain boundaries

3.2.2. *Electropolishing*. Though I did not perform any electropolishing and did not investigate the technique very thoroughly, I will provide an SEM image (Figure 23) from a paper of RL Geng *et al* [12] for the sake of comparison. This image shows a sample which was first etched in BCP to remove 117 µm, then electropolished to remove an additional 90 µm. The sharpness of the BCP grain boundaries has been greatly smoothed away. The length scale bar is 100 µm.

[12] R L Geng, J Knobloch, H Padamsee, Microstructures of RF Surfaces on the Electron-Beam-Weld Regions of Niobium, *Proc. of the 9th Workshop on RF Superconductivity*, Santa Fe, NM (1999).

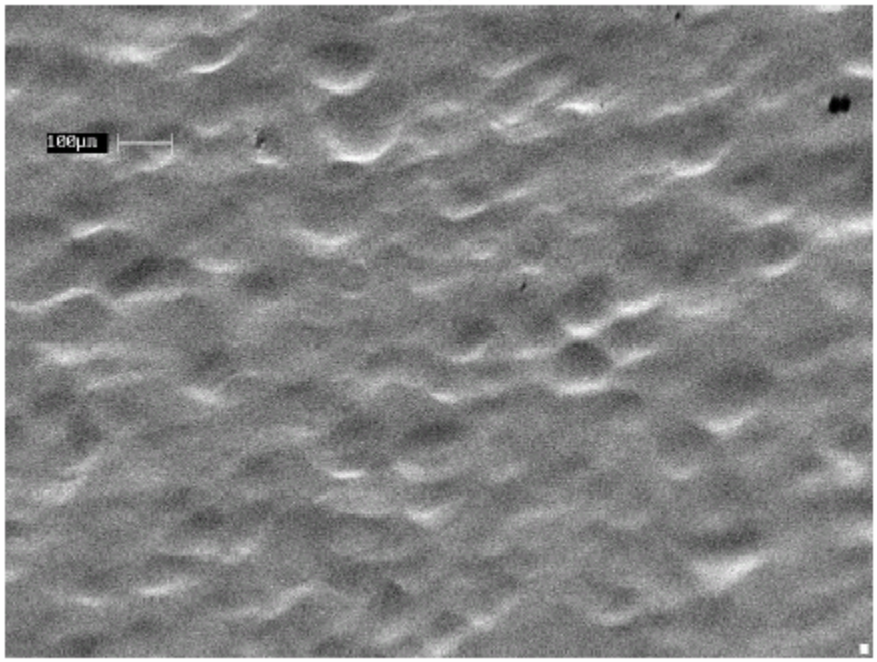

Figure 23: SEM image of electropolished niobium

3.2.3. *BCP 1:1:1.* I also examined BCP in a different recipe from that which is most commonly used, as a first experiment. The SEM images are essentially indistinguishable from BCP 1:1:2 (Figure 21), and the grain boundaries look similar under the AFM as well. This is in accordance with the result found in [3].

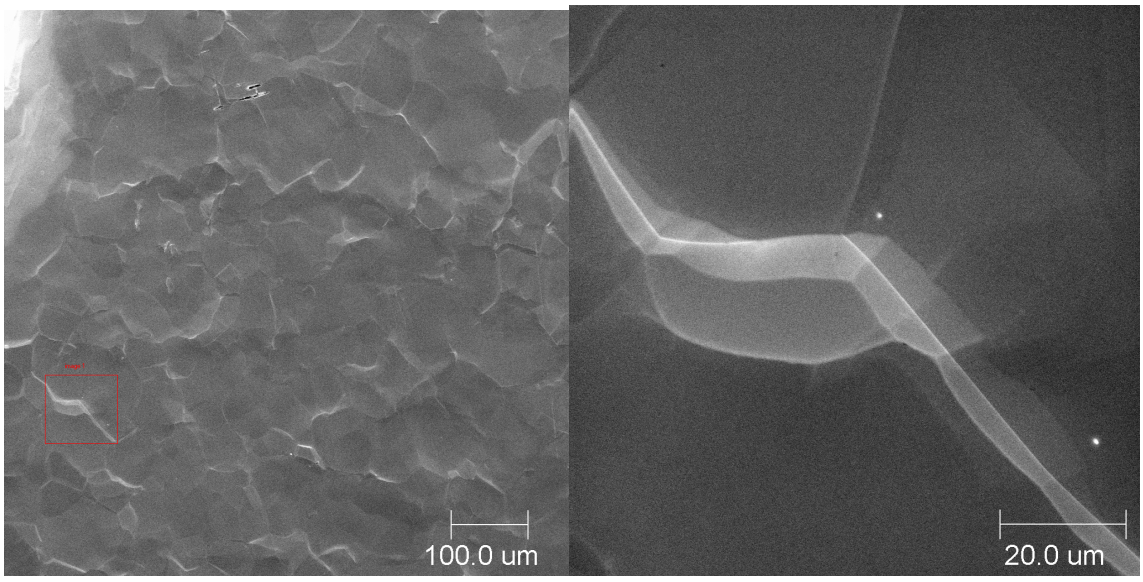

Figure 24: SEM images of RRR 300 niobium etched in BCP 1:1:1

3.2.4. *RRR 300 FNS 1:1:1*: Next, a 300 RRR niobium sample which had undergone a surface removal of 120µm in FNS 1:1:1 was examined. In comparison to the BCP, this sample shows a strange range of surface features under the SEM (Figure 25).

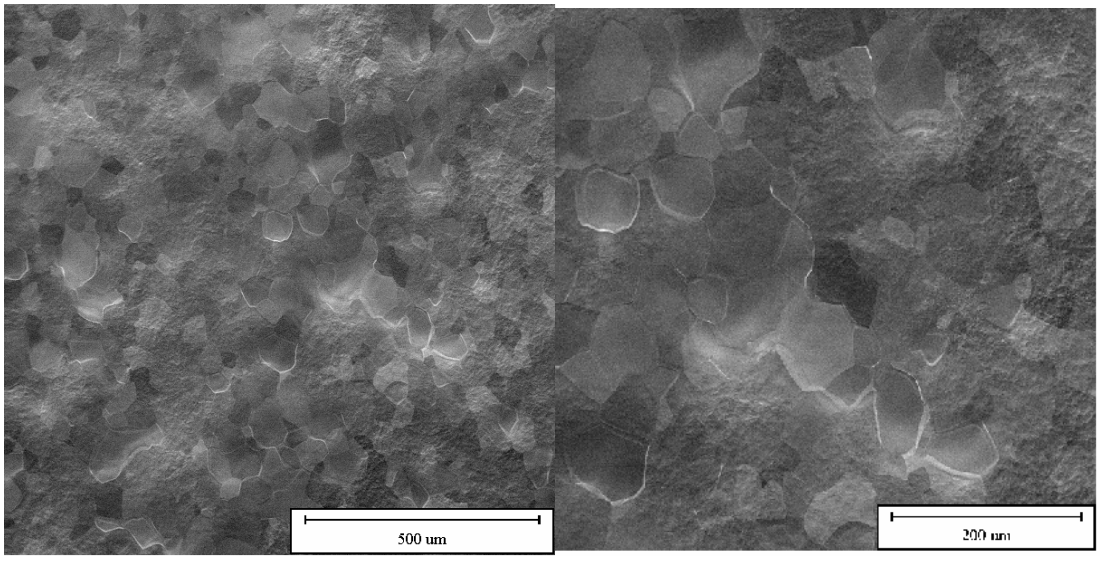

Figure 25: SEM image of 300 RRR FNS 1:1:1 sample. The scale bar on the left is 500µm, and on the right (a closeup image) is 200µm.

First, note that large-scale variations can be seen in the larger-scale image, and seem to manifest as areas of smoothness and roughness in the smaller-scale image. Figure 26 contains close-up images of grain boundaries, including some in "flat" and some in "rough" regions. As compared to the BCP grain boundaries, the steps in these images do appear to be less severe or tall; however, the rough areas may be problematic and the large scale structure is puzzling.

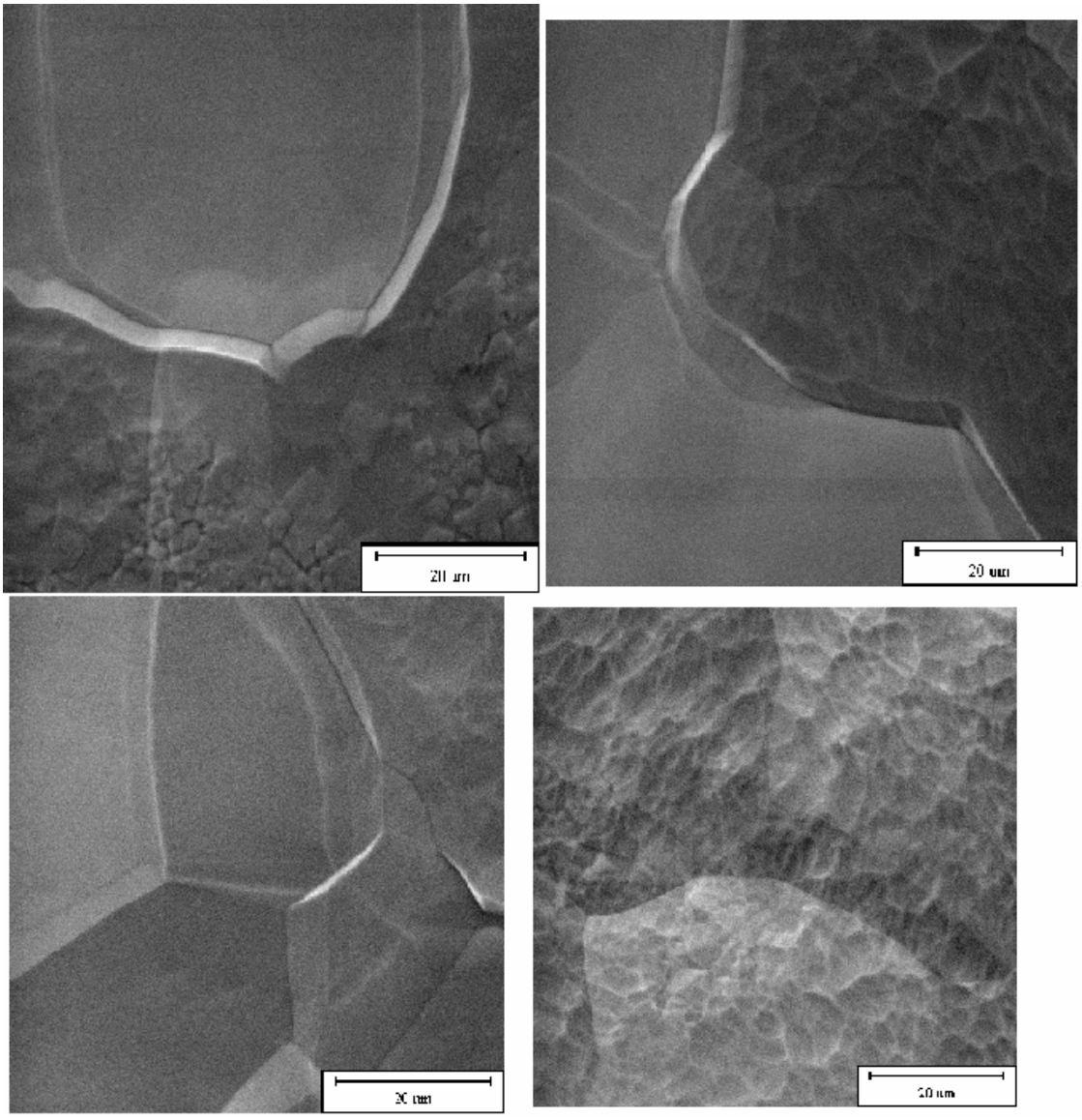

Figure 26: FNS 1:1:1 grain boundary closeups. All scale bars are 20µm.

AFM measurements, however, show that the features that remain are still sharp. Sharper (as measured by their angle measurements), in fact, than the BCP samples (see Figure 27). It seems that the vertical size of the steps may be reduced (as compared to BCP) but the sharpness of the boundaries may increase.

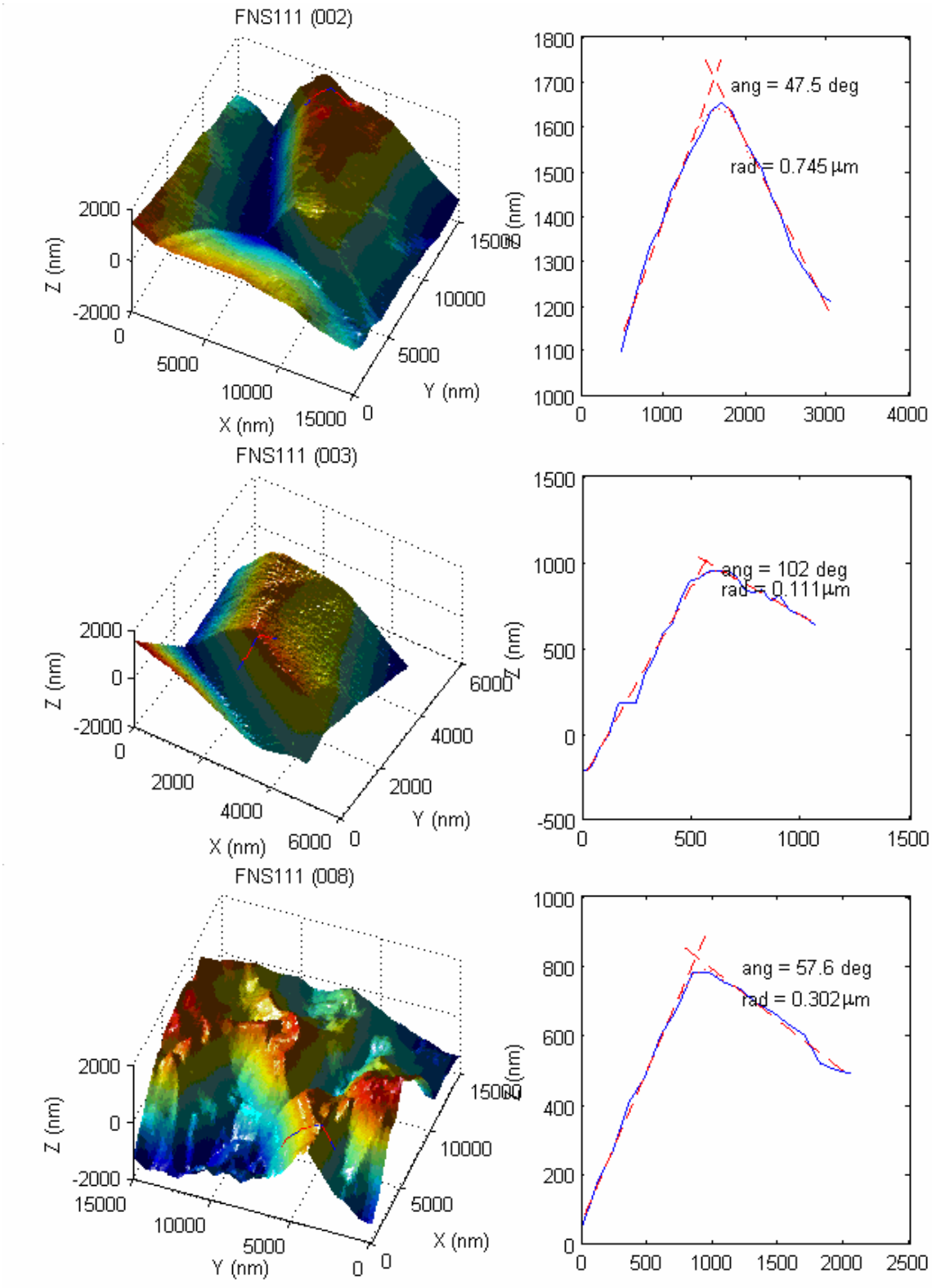
FNS111 (002)
Z (nm)
X (nm)
Y (nm)
ang = 47.5 deg
rad = 0.745 µm
FNS111 (003)
ang = 102 deg
rad = 0.111µm
FNS111 (008)
ang = 57.6 deg
rad = 0.302µm

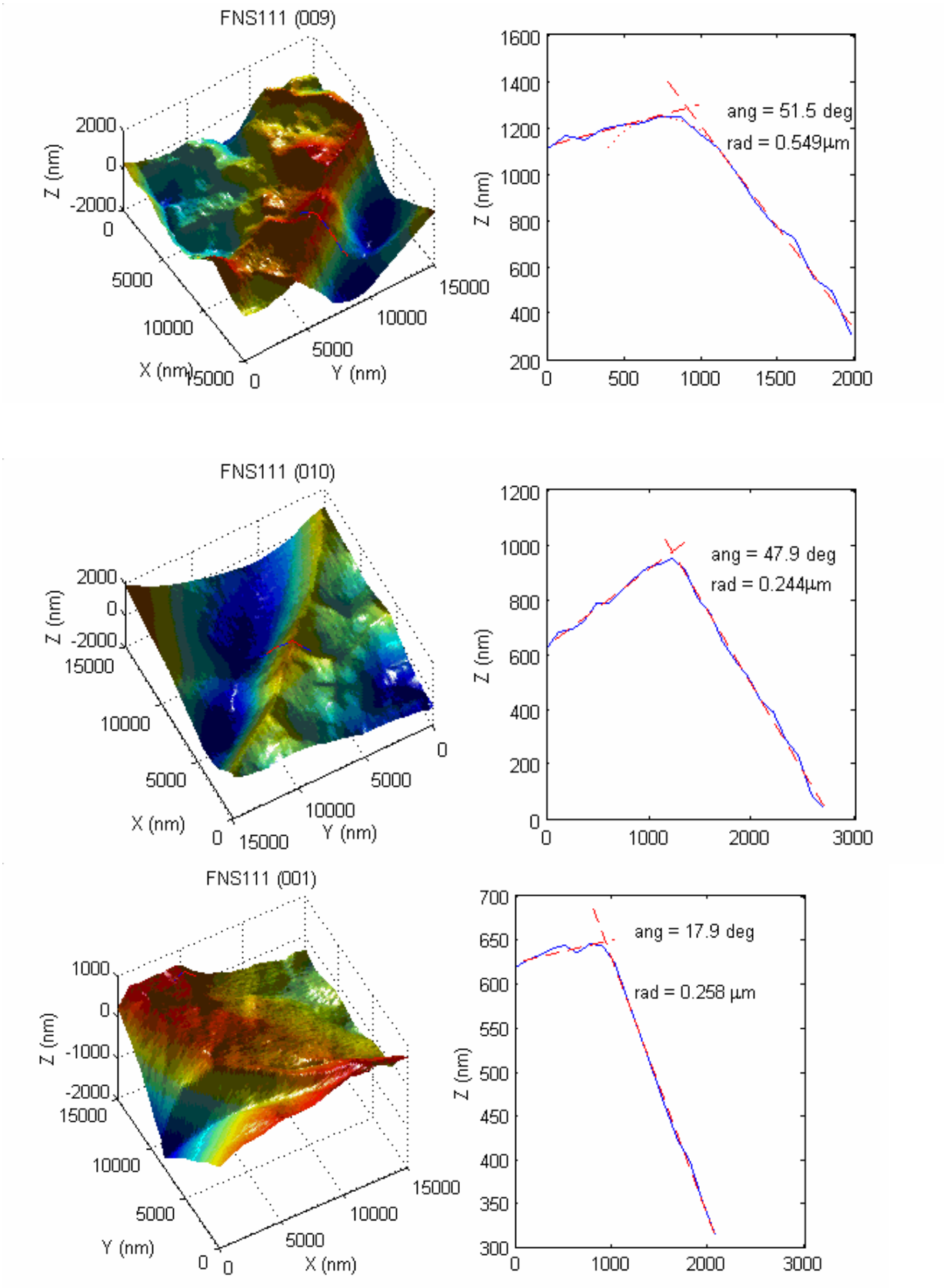

Figure 27: AFM images of FNS 1:1:1 grain boundaries

3.2.5. *RRR 500 FNS 1:1:1:* Polishing using the FNS 1:1:1 recipe was also performed on higher purity (RRR 500) niobium. The SEM images (Figure 28) look very similar to the 300RRR sample (Figure 25). Note also how in the lower left image in Figure 28, it seems that a grain boundary has been almost completely worn away by the polishing. AFM measurements (Figure 29) seem to show a generally more rounded surface, however, and fewer extremely-shaped ridges (though it is, of course, hard to be sure with the small number of images taken).

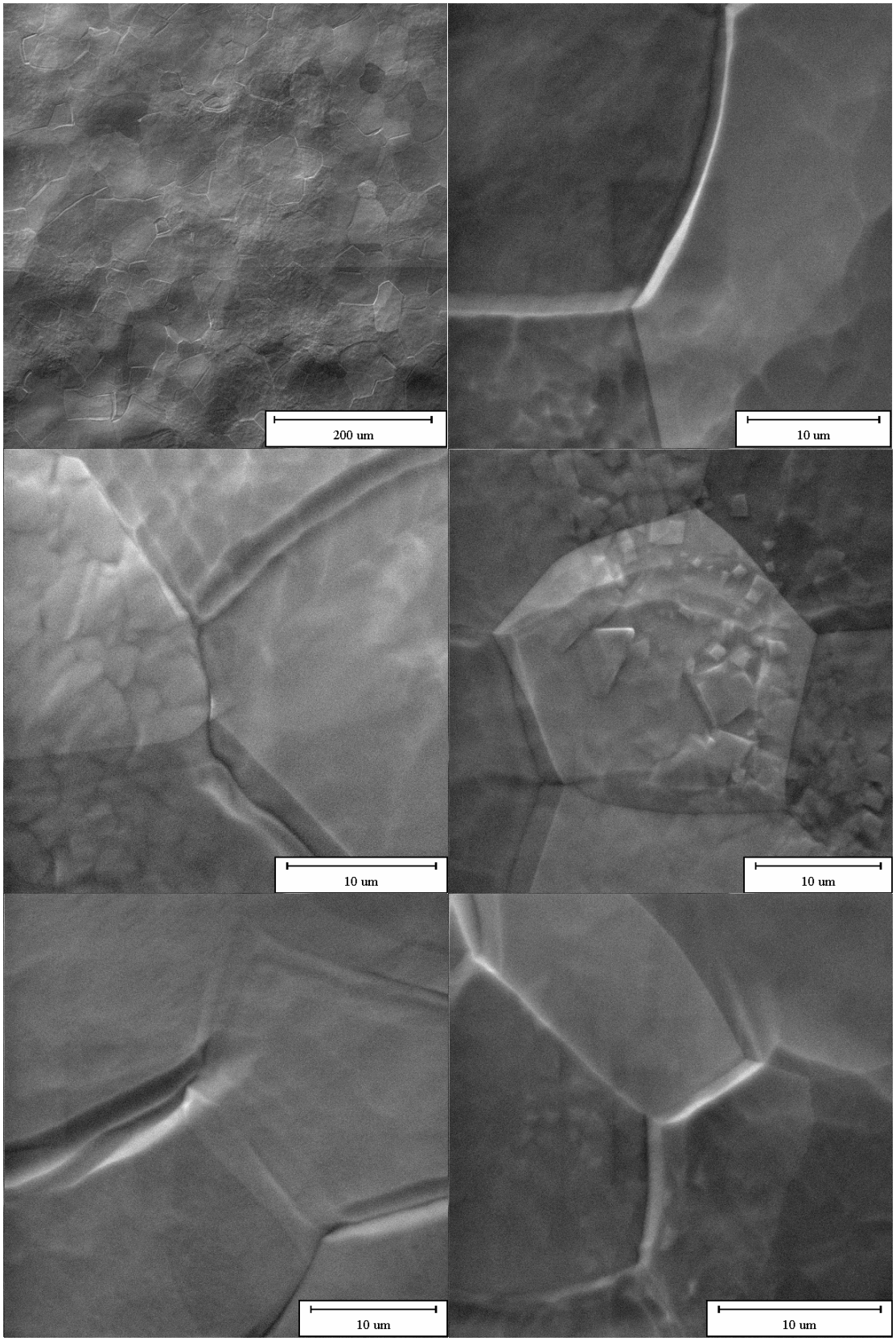

Figure 28: SEM images of 500RRR niobium etched in FNS 1:1:1.

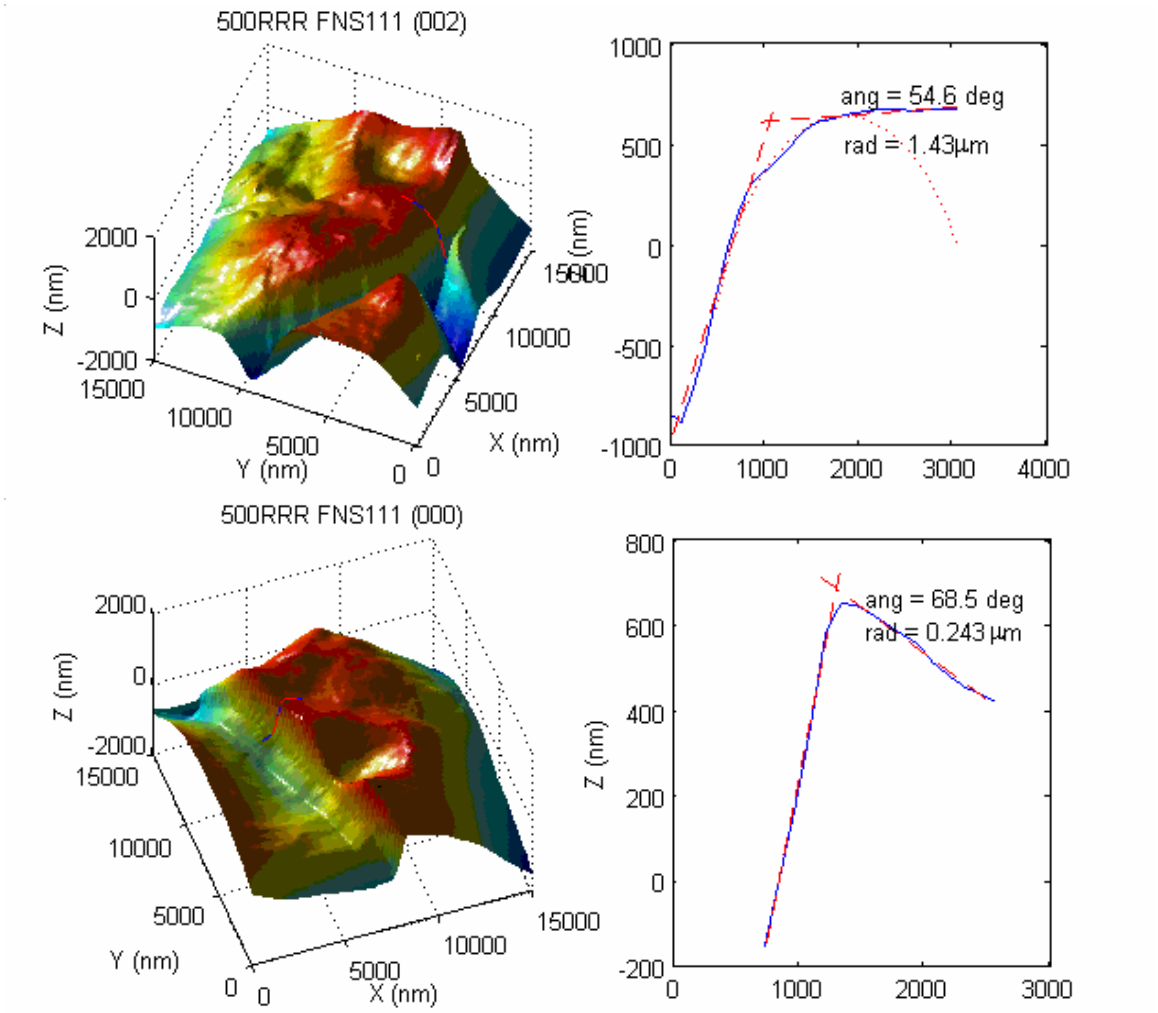

Figure 29: AFM images of RRR 500 niobium etched in FNS 1:1:1

3.2.6. *RRR 500 FNS 112:* I thought that it was worth looking at the effects of a recipe FNS 1:1:2, though the literature had only mentioned FNS 1:1:1. The results are noticeably different from either the BCP or the FNS 1:1:1 results. SEM images (Figure 30) show very sharp grain boundaries. The sample did seem to have less of the large-scale structure observed in the FNS 1:1:1 samples, but there were curious new features in the form of “bubbles” (see lower left image) at

some places in the sample. AFM measurements (Figure 31) confirm the sharpness of the grain boundaries.

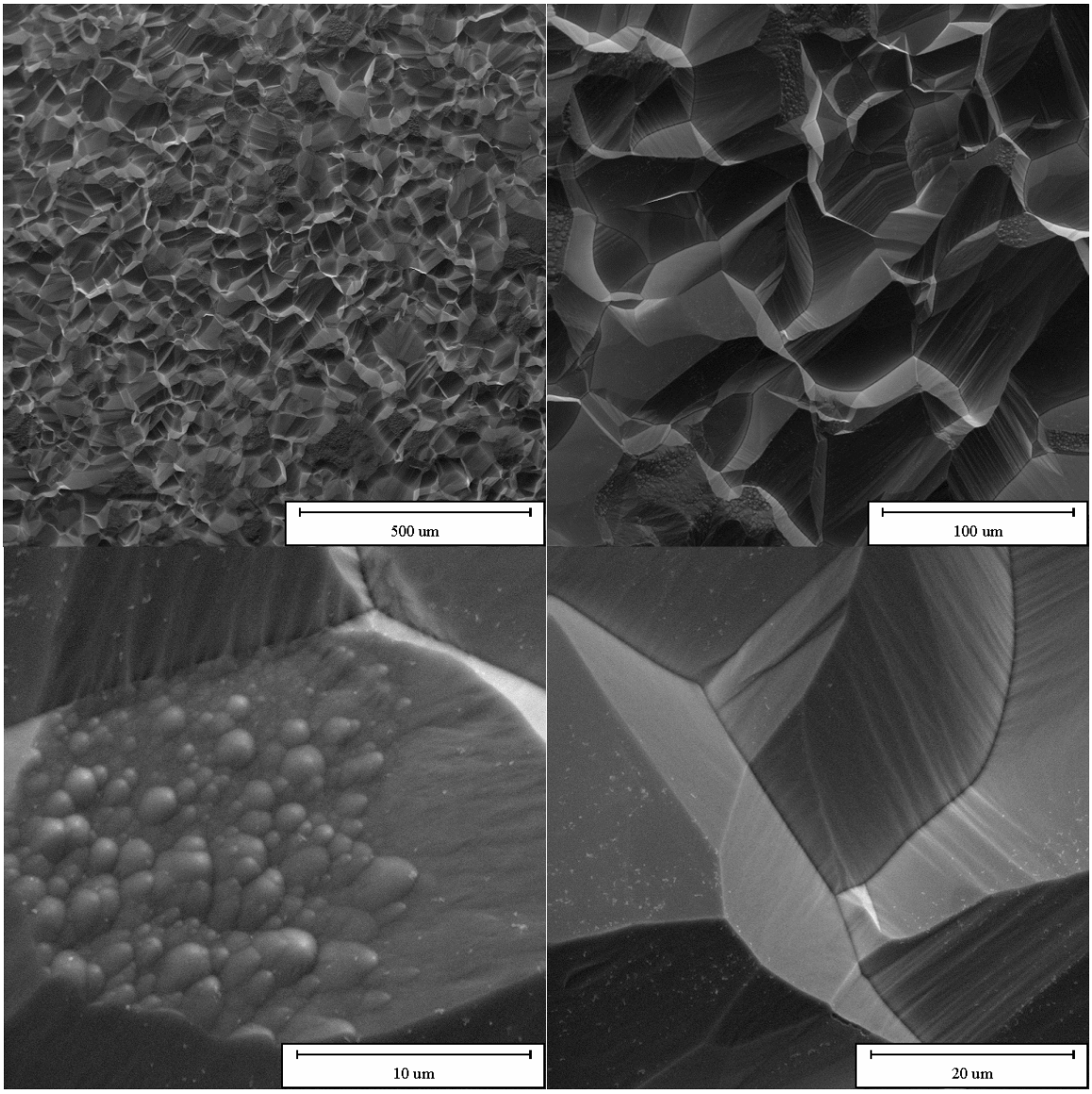

Figure 30: SEM images of RRR 500 niobium etched in FNS 1:1:2

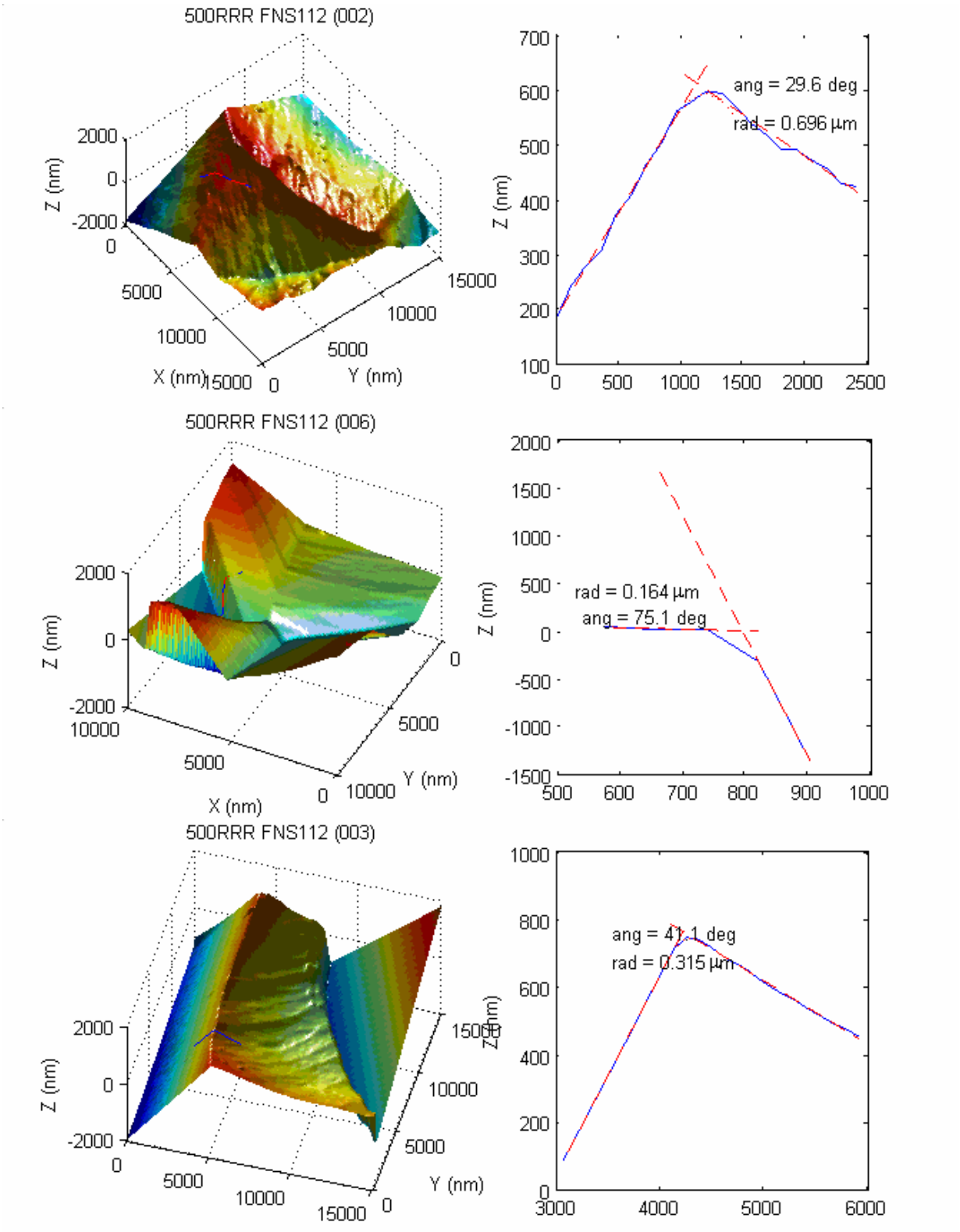

Figure 31: AFM images of RRR 500 niobium etched in FNS 1:1:2

3.2.7. *RRR 500 BCP 1:1:2:* The higher purity niobium etched in BCP 1:1:2 is an interesting sample. SEM images (Figure 33) show that it is markedly different from BCP 1:1:2 on the RRR 300 niobium (Figure 21, comparison Figure 32), and AFM images (Figure 34 and Figure 35) also show this difference. It is hard to find an AFM image of a grain boundary on this sample with an angle of more than 10 or 15 degrees, whereas these are quite common on the 300 RRR sample. The comparison image (Figure 32) also shows that the grain size on the RRR 500 niobium seems to be slightly smaller.

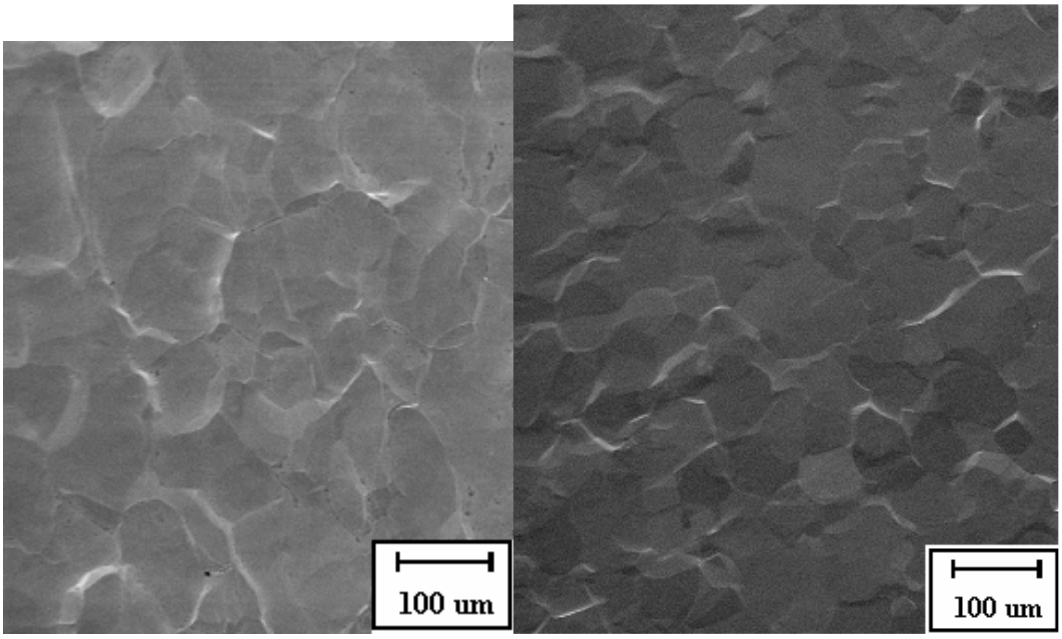

Figure 32: Comparison of 300 RRR (left) and 500 RRR (right) niobium samples etched in BCP 1:1:2

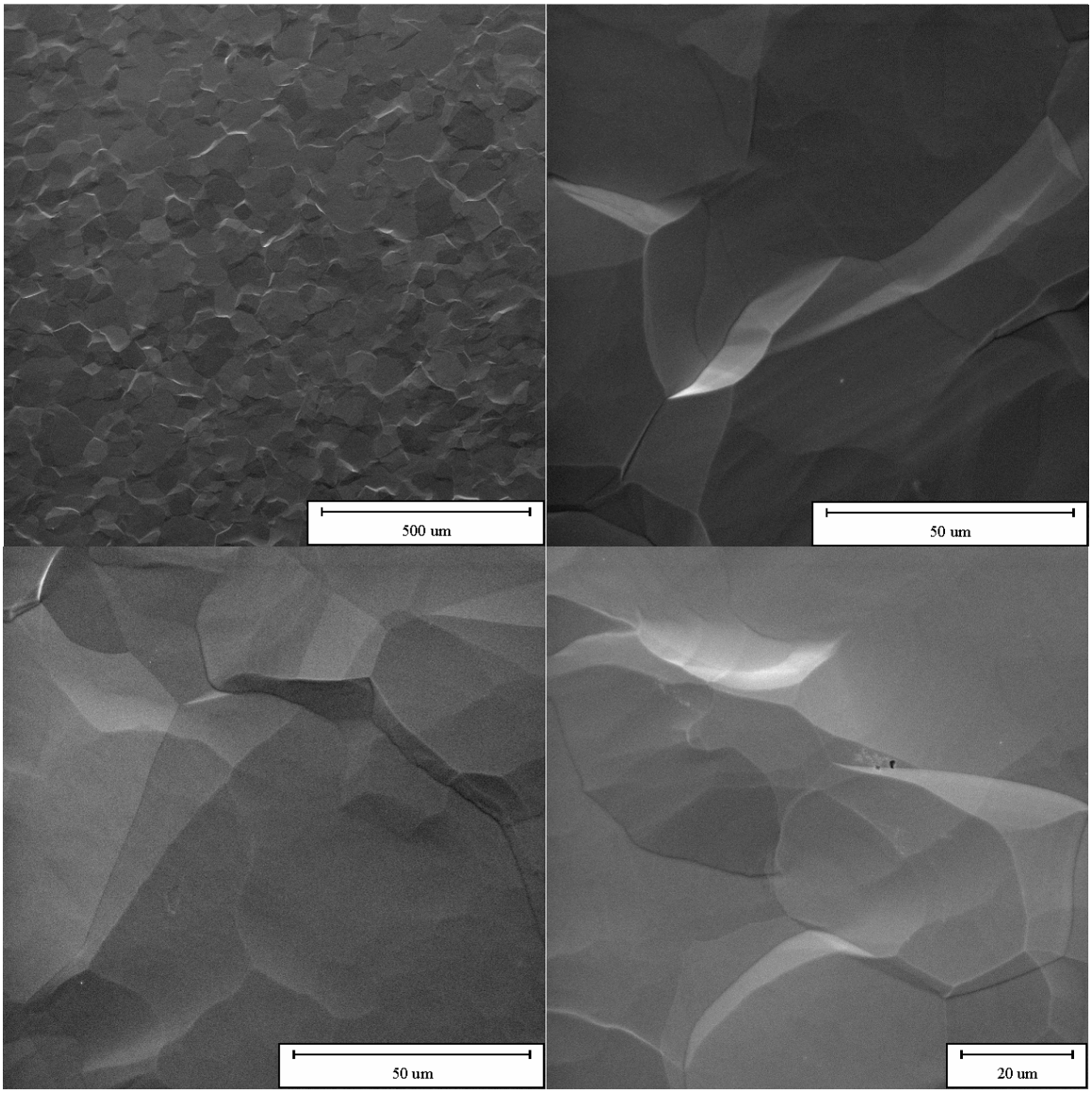

Figure 33: SEM images of RRR 500 niobium etched in BCP 1:1:2

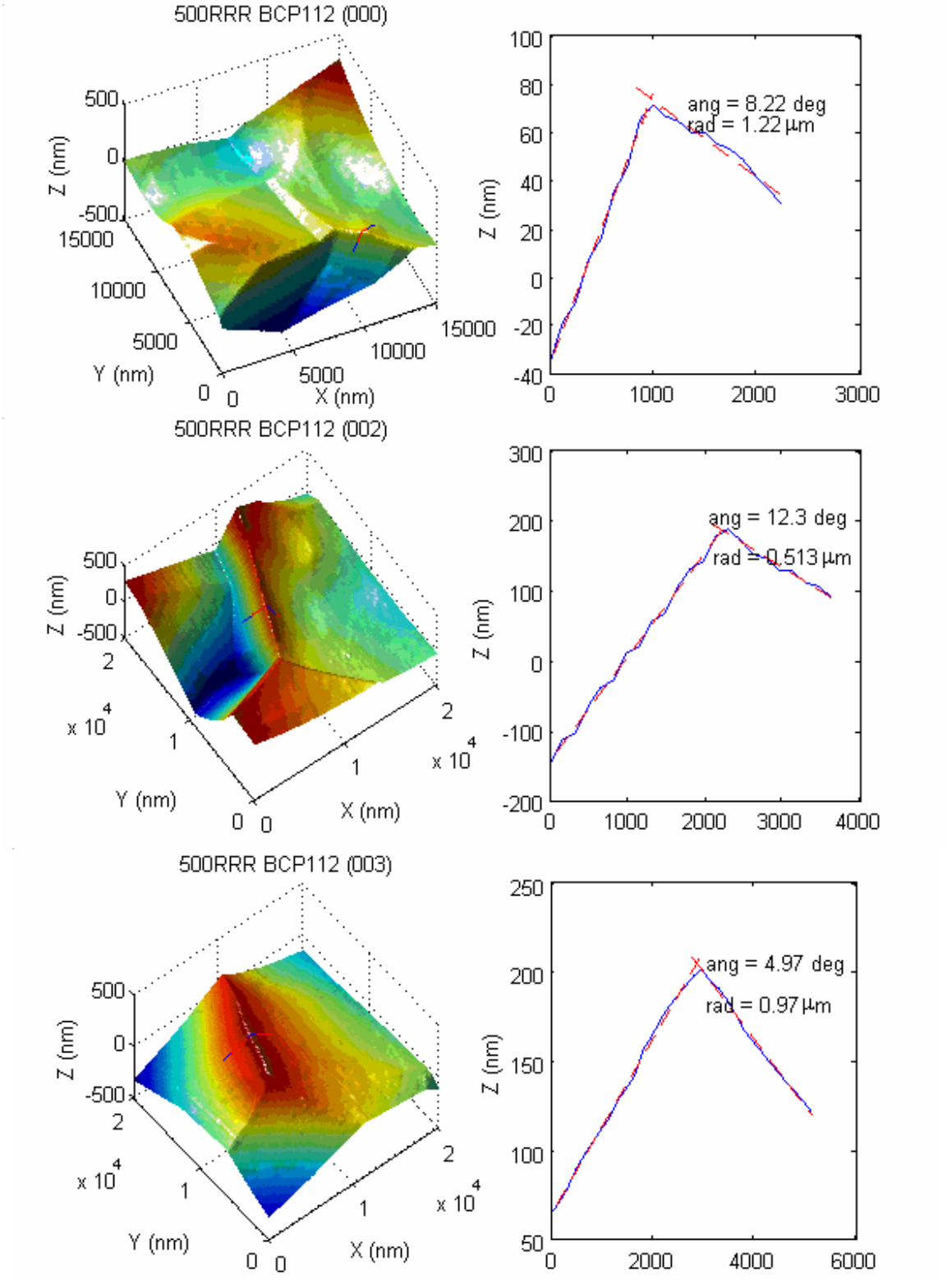

Figure 34: AFM images of 500 RRR niobium etched in BCP 1:1:2

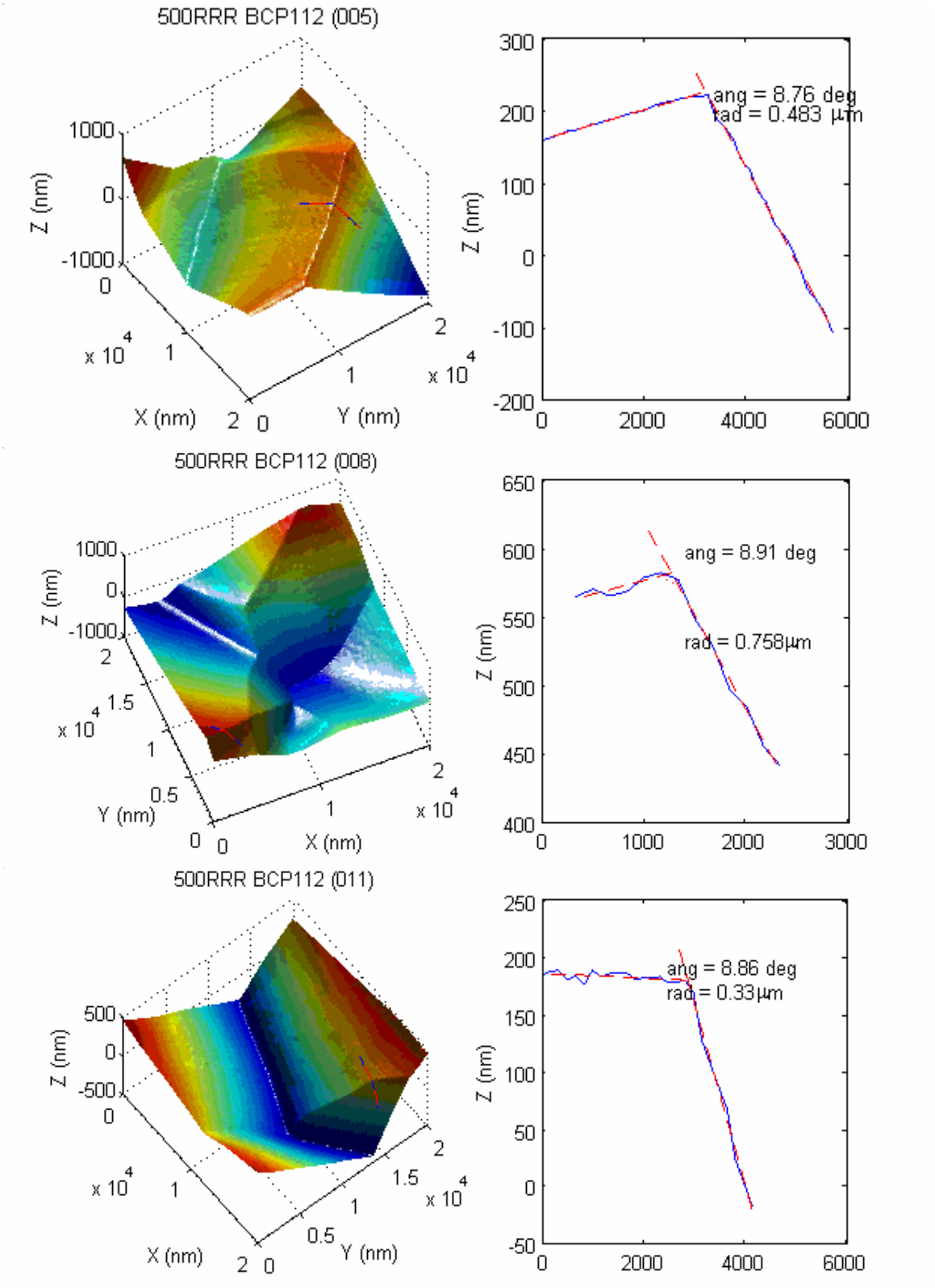

Figure 35: More AFM images of grain boundaries on RRR 500 niobium etched in BCP 1:1:2

3.2.8. *RRR 500 BCP 1:1:1:* I also examined a high purity niobium sample which had been etched in BCP 1:1:1. It looked very much like the high purity BCP 1:1:2 sample, above. Figure 36 shows some examples.

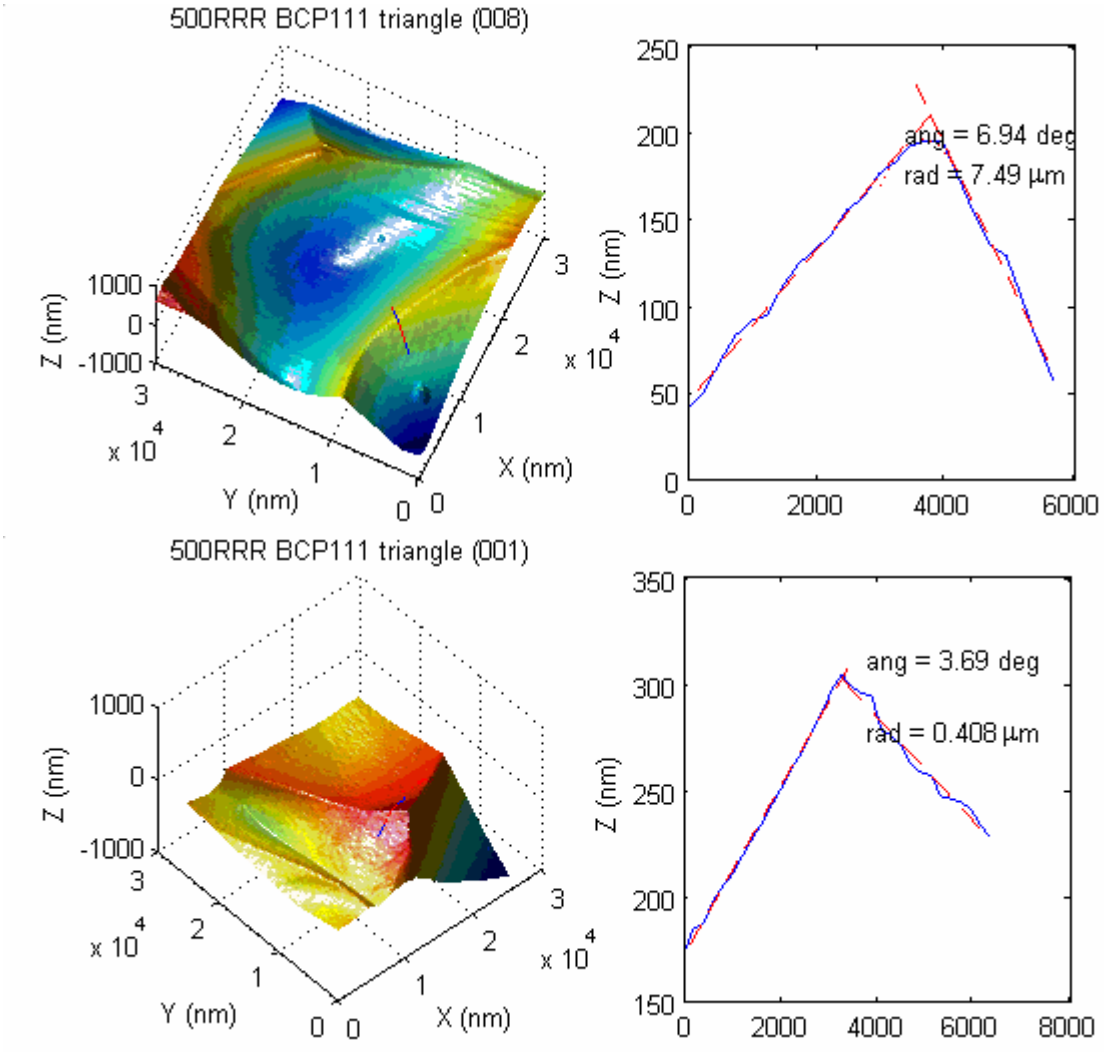

Figure 36: AFM images of high purity niobium etched in BCP 1:1:1

3.2.9. *Oxypolishing*: I oxypolished both a BCP 1:1:1 sample and a 500 RRR BCP 1:1:2 sample. In the case of the BCP 1:1:1, a total of 510 V (over 6

cycles) were anodized; for the higher purity sample, a total of 380 V (over 4 cycles) were anodized. These correspond to 1.0 and 0.76 microns of oxide, respectively. SEM images looked very similar to the pre-oxypolishing images, except that some small-scale features were introduced and were barely noticeable but hard to investigate well. AFM images (Figure 37) show small craters and other imperfections. The angles and radii of curvature were not profoundly different from pre-processed measurements.

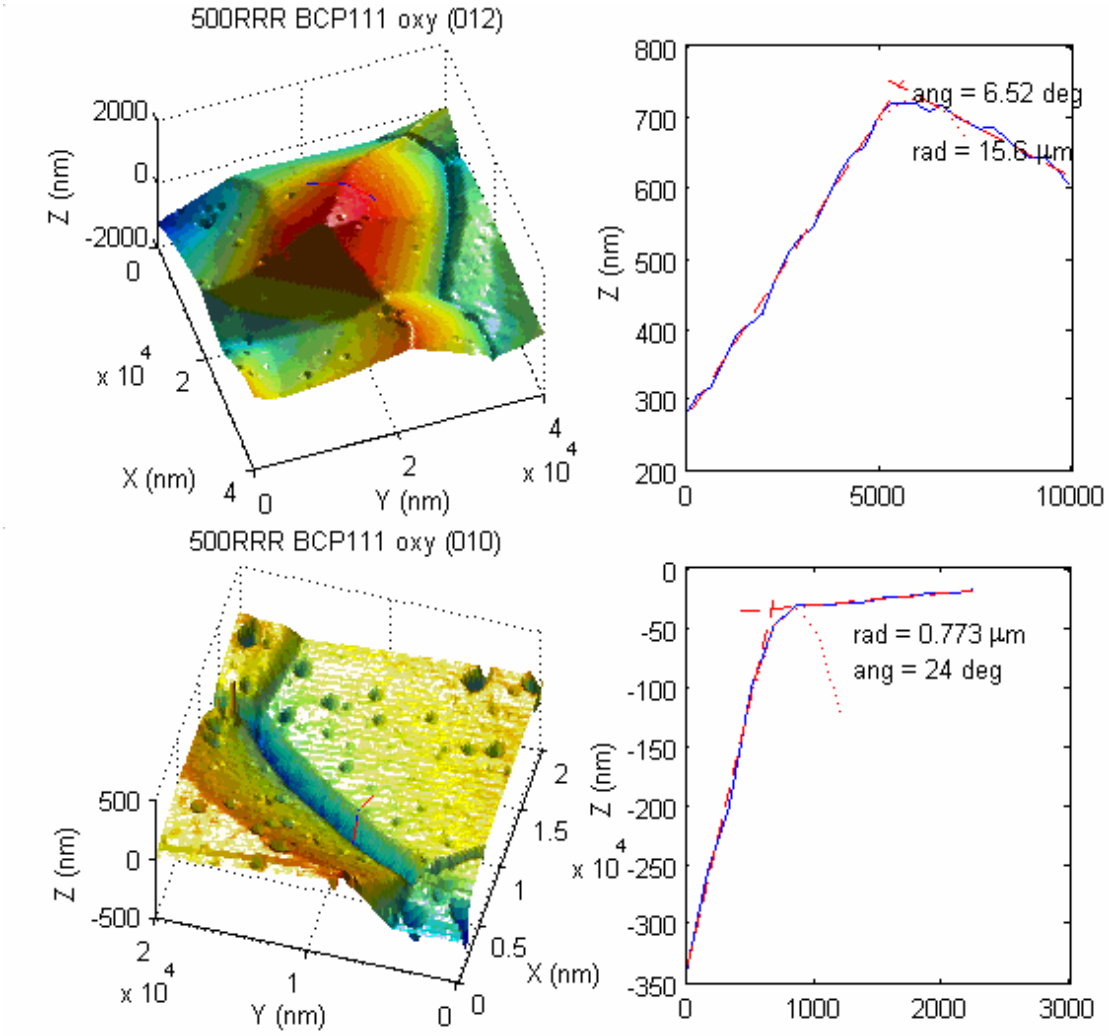

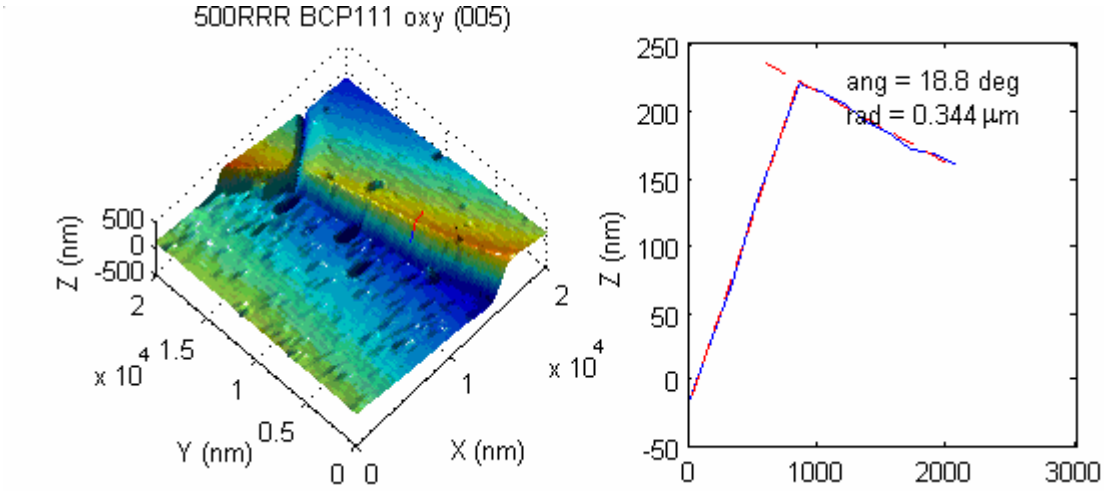

Figure 37: AFM images of oxypolished samples

3.2.10. *Gas Cluster Ion Bombardment*: GCIB was performed on RRR 300 niobium which had been etched in BCP 1:1:2. Five pedestals about 2 mm high were machined into the sample in order to facilitate trying a variety of different GCIB treatments (Figure 38). One of the pedestals (#5) was left unprocessed by GCIB for the sake of comparison. The other four were processed with different species of gas.

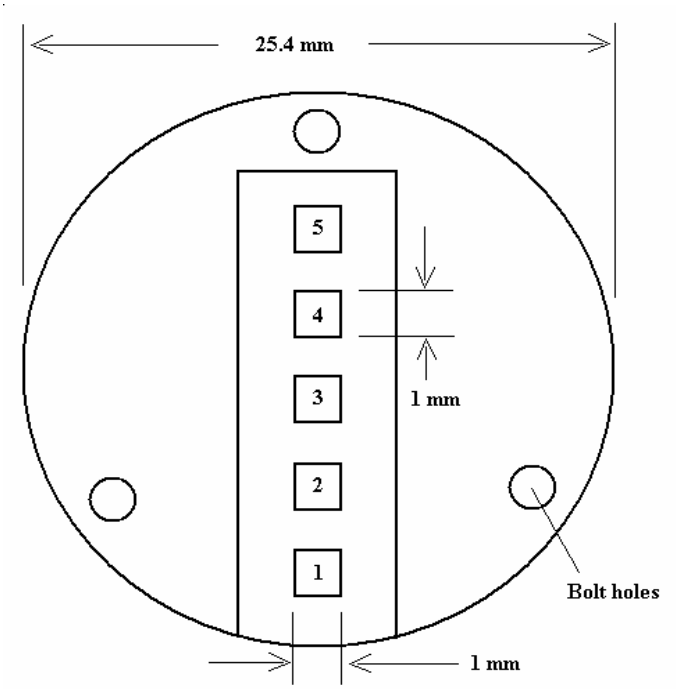

Figure 38: Niobium sample with five pedestals (not to scale)

3.2.10.1. Pedestal 4 - GCIB with Ar: The pedestal (Figure 39) looks similar to standard BCP etch (Figure 21 or Figure 24), and some of the grain boundaries (Figure 40, left) look similar as well. However, some regions (Figure 40, right) have been smoothed out noticeably. AFM images (Figure 41) are similar to those of other BCP samples.

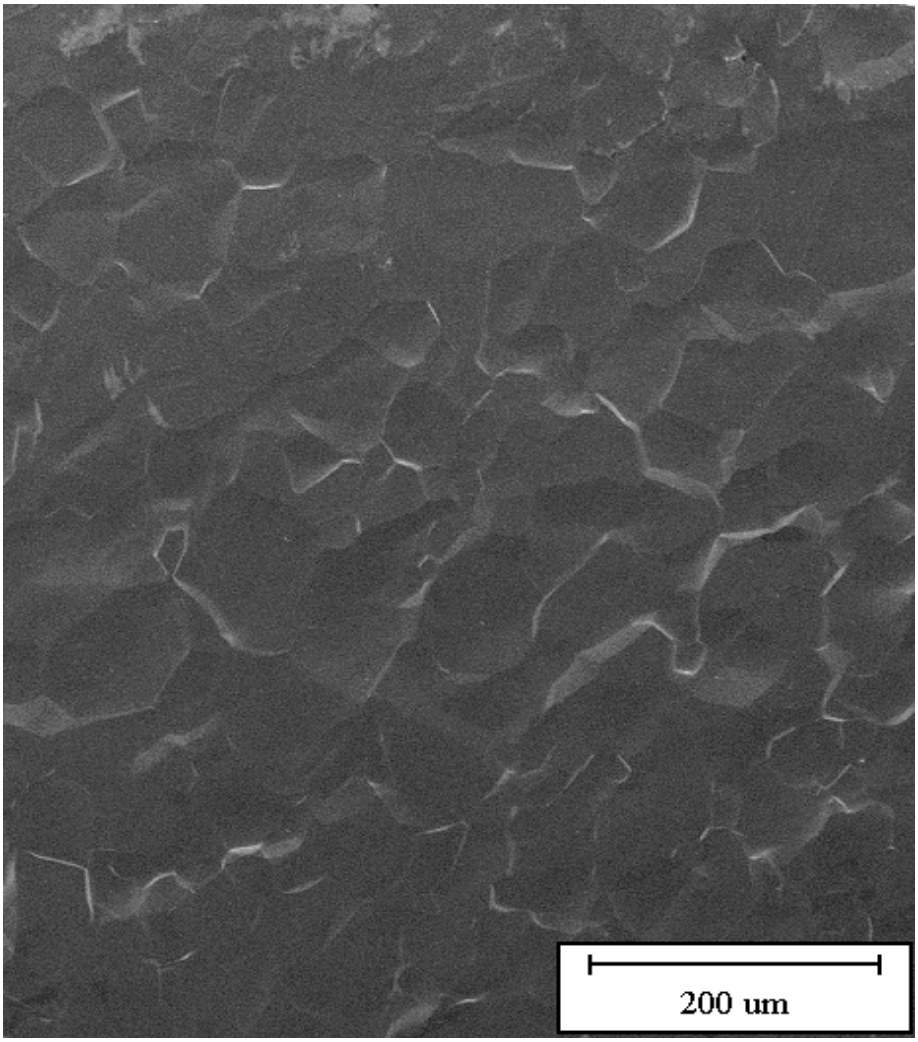

Figure 39: SEM image of the niobium pedestal processed with argon GCIB

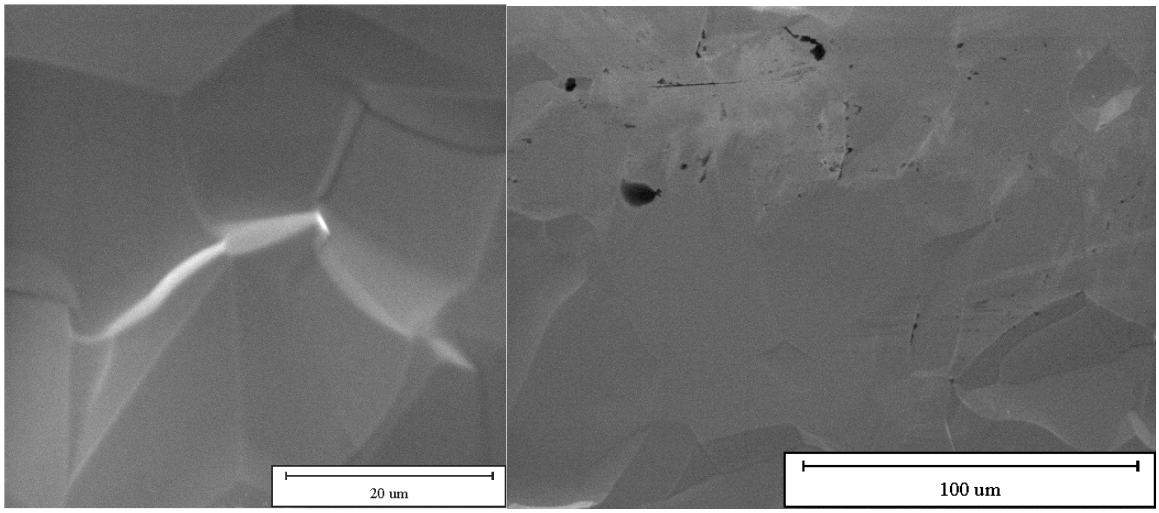

Figure 40: SEM close-ups of a (left) seemingly less-affected region and a (right) seemingly more-affected region after argon GCIB processing.

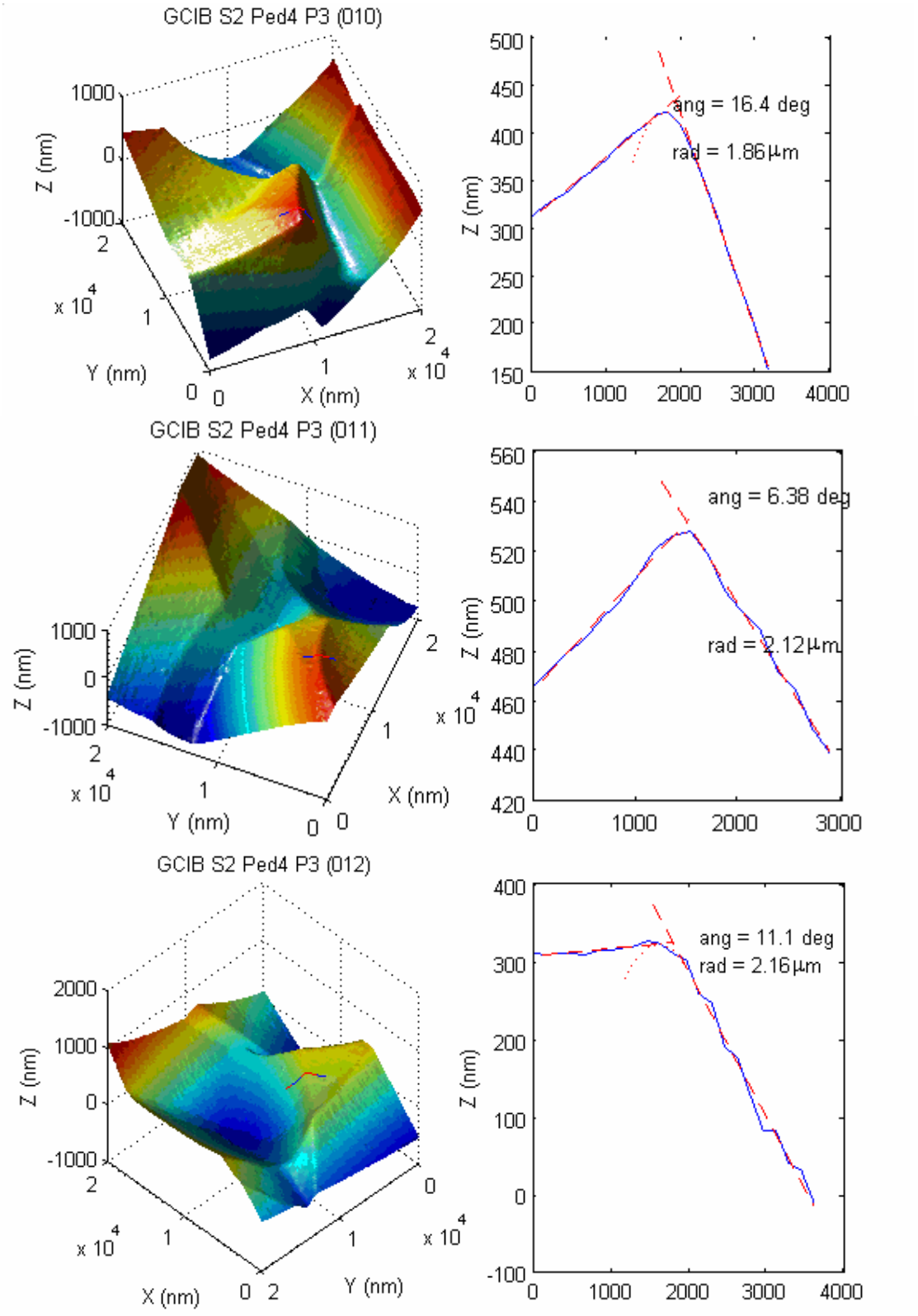

Figure 41: AFM images of niobium after Ar GCIB processing

3.2.10.2. Pedestal 3 – GCIB with argon and hydrogen gas: The pedestal (Figure 42) does look somewhat different from other BCP samples. It is as if the contrast in the image has been reduced. Since the samples were examined in the SEM at a slight tilt (8°) to bring out the grain boundaries and other topographic features, the contrast does have something to do with the height and sharpness of grain boundaries. Still, as with the other GCIB pedestals, there seem to be more affected and less affected regions (Figure 43, left and right respectively). AFM measurements (Figure 44) also suggest that the grain boundaries are somewhat more rounded than BCP samples unprocessed with GCIB.

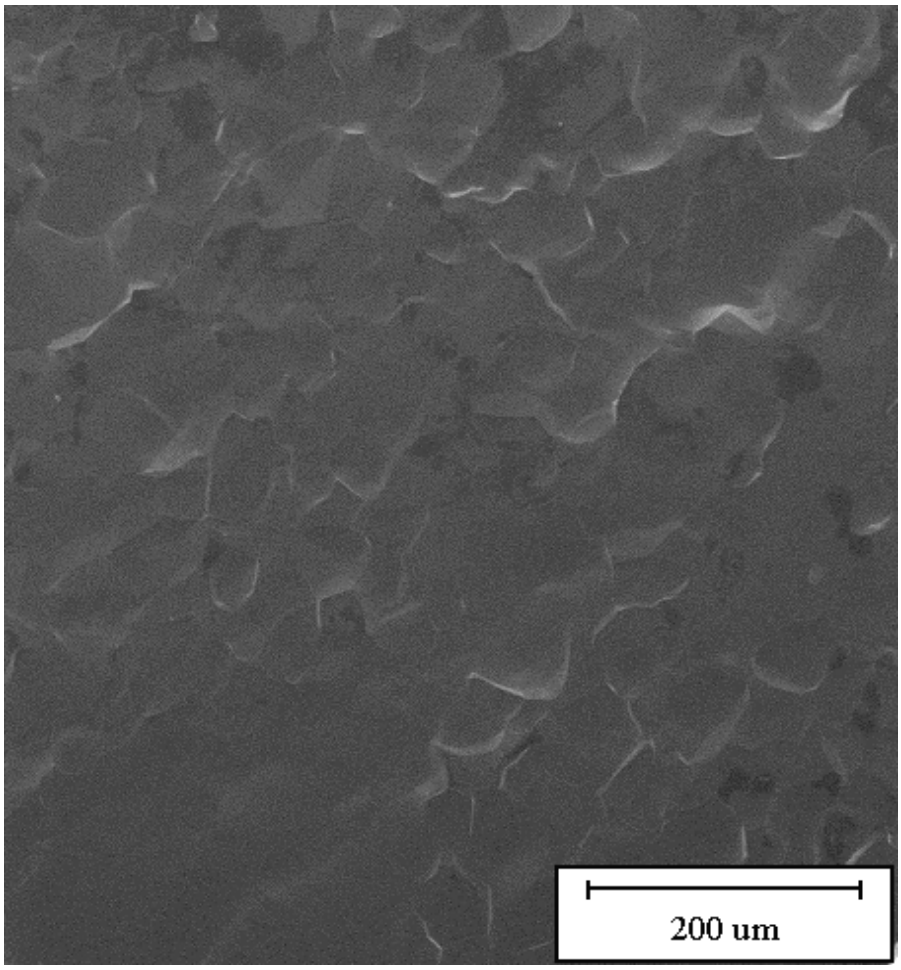

Figure 42: SEM image of niobium pedestal processed with Ar and H_2 GCIB

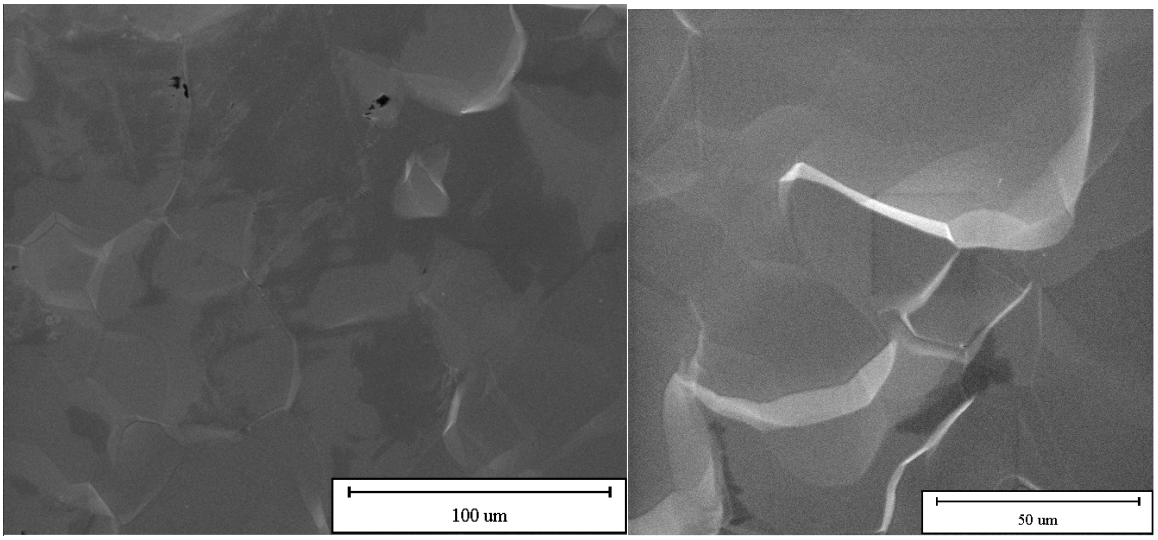

Figure 43: SEM close-ups of seemingly more-affected and less-affected regions on Ar + H_2 GCIB sample

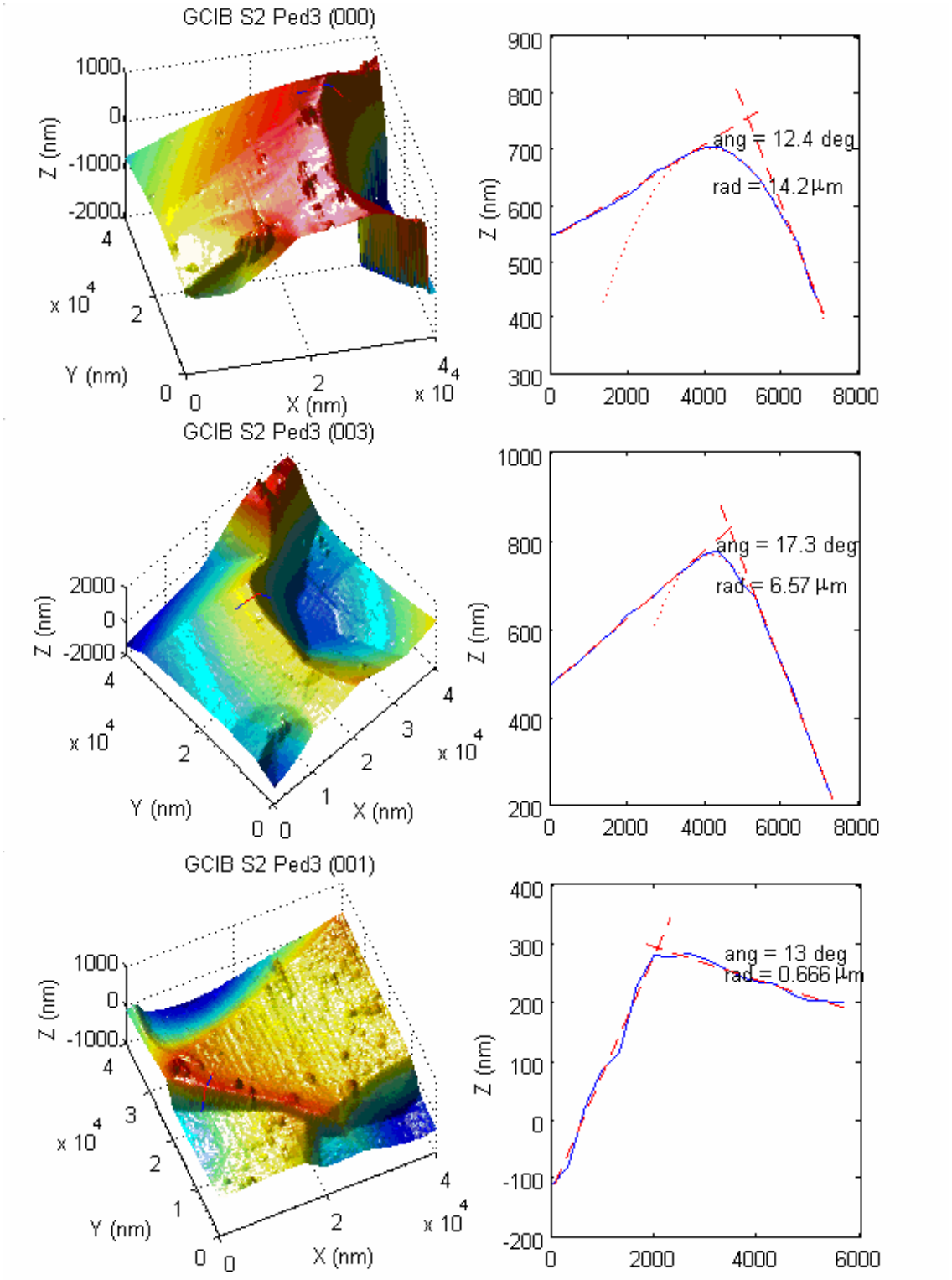

Figure 44: AFM images of grains processed with Ar + H_2 GCIB

3.2.10.3. Pedestal 2 – GCIB with argon and methane (CH_4): This pedestal looked under the SEM (Figure 45) to be somewhat dirty, as if it had scuffed up against something. Seeing this, I figured that it was less valuable to spend a lot of time looking at it, but took several grain boundary measurements with the AFM (Figure 46) just in case anything drastic turned up.

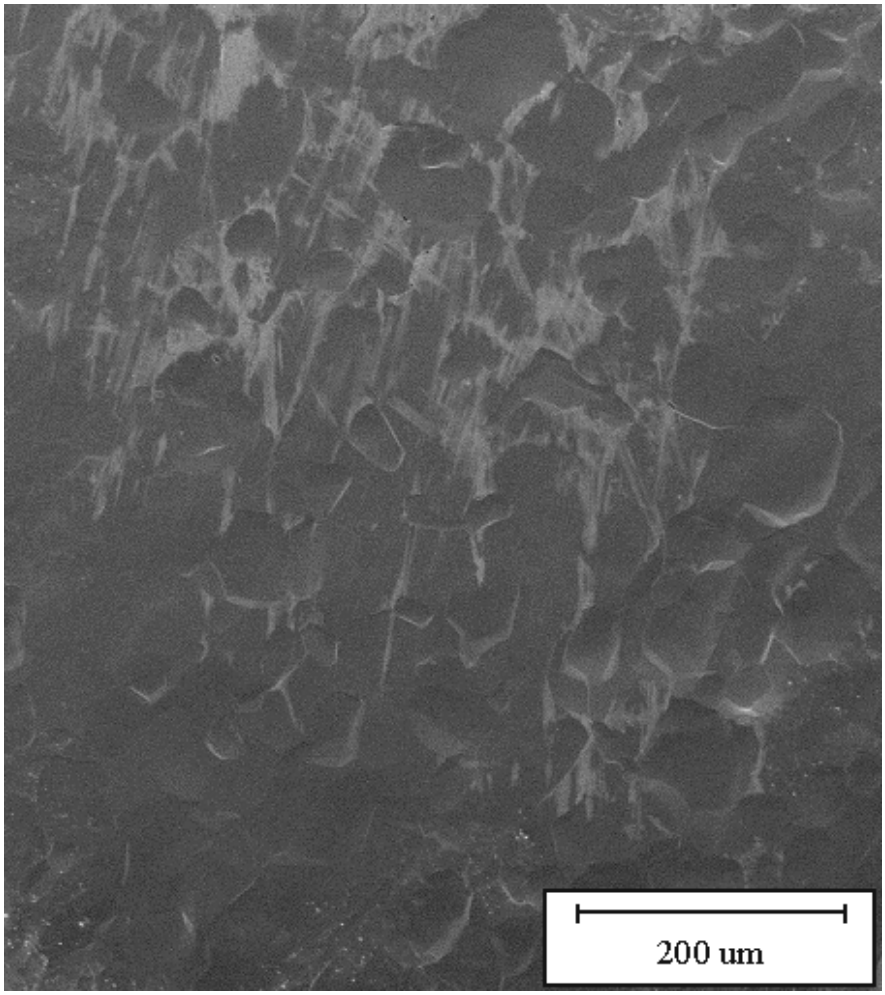

Figure 45: Pedestal processed with Ar + CH_4 GCIB; looks as if it were rubbed up against something?

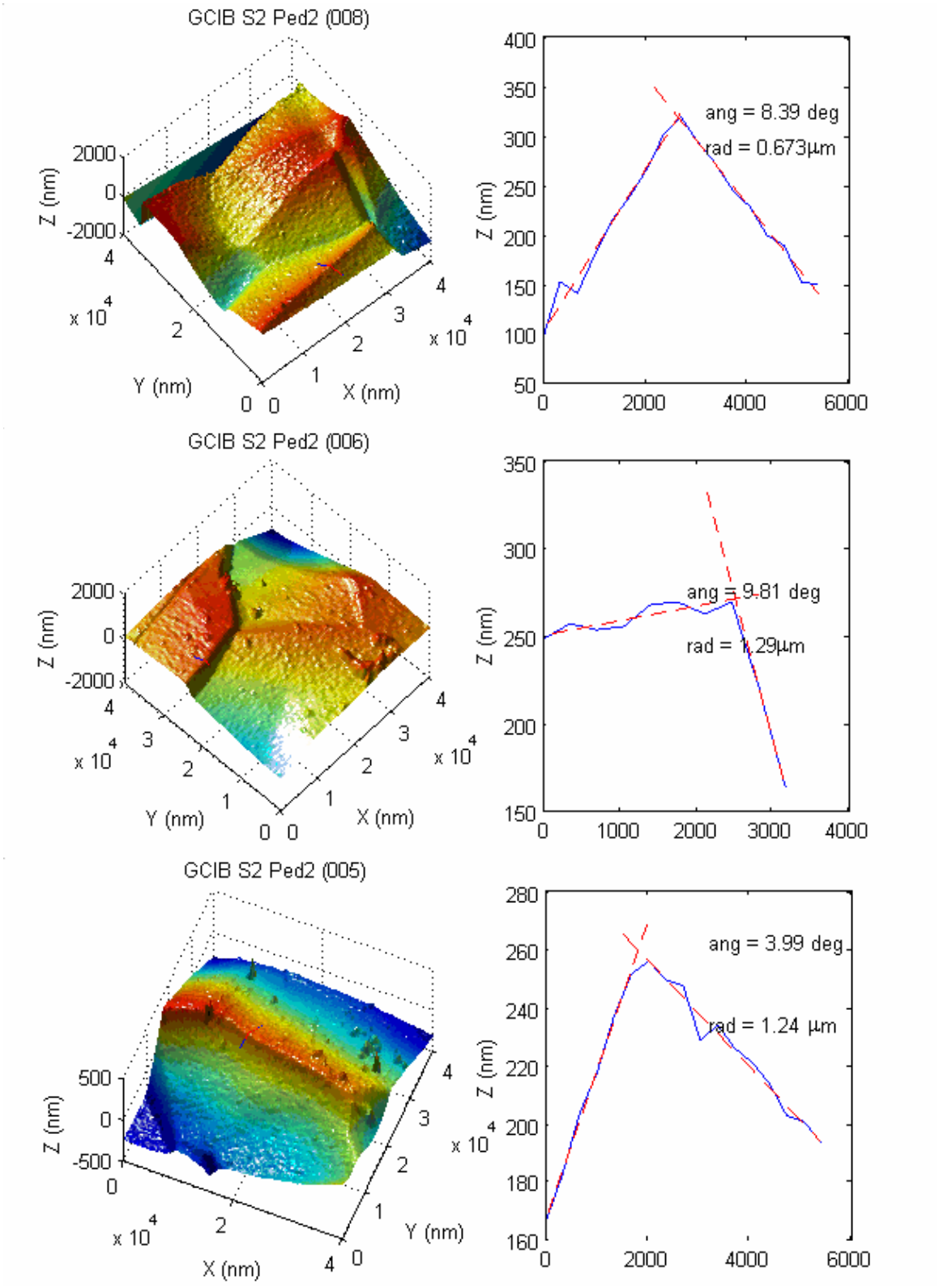

Figure 46: AFM images of niobium processed with Ar + CH_4 GCIB

3.2.10.4. Pedestal 1 – GCIB with NF_3 and O_2: The final GCIB process I examined had a dramatic effect on the look of the pedestal in the SEM (Figure 47). While again there seemed to be more- and less- affected regions, grain boundaries across the board did not resemble ordinary BCP grain boundaries. They were generally much reduced in the z-dimension and AFM measurements found that the angles seemed to be smaller, accordingly.

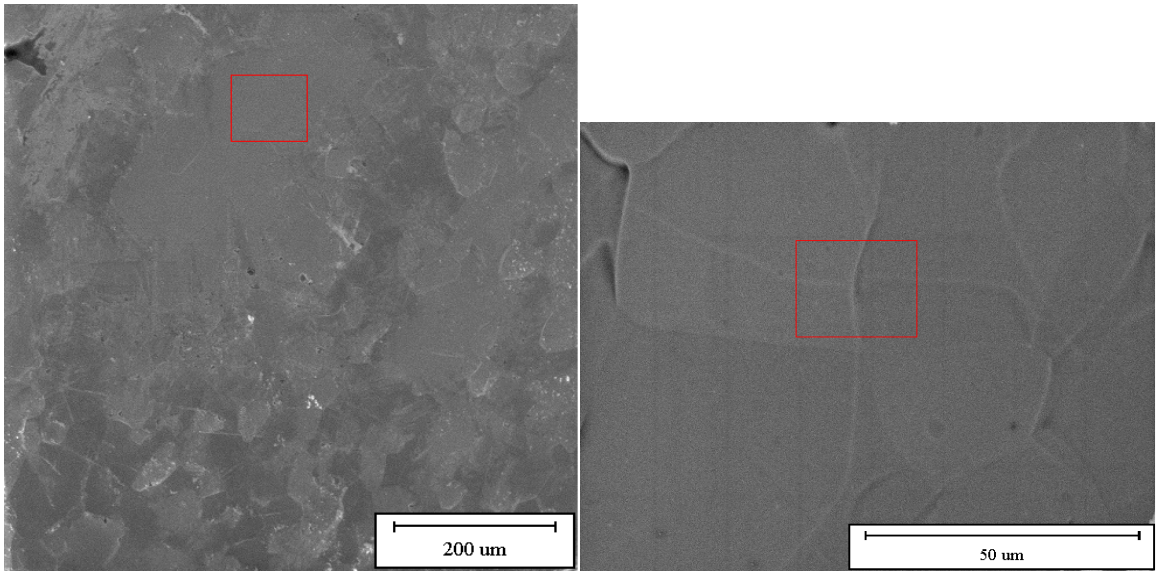

Figure 47: SEM images of niobium processed with NF_3 + O_2 GCIB

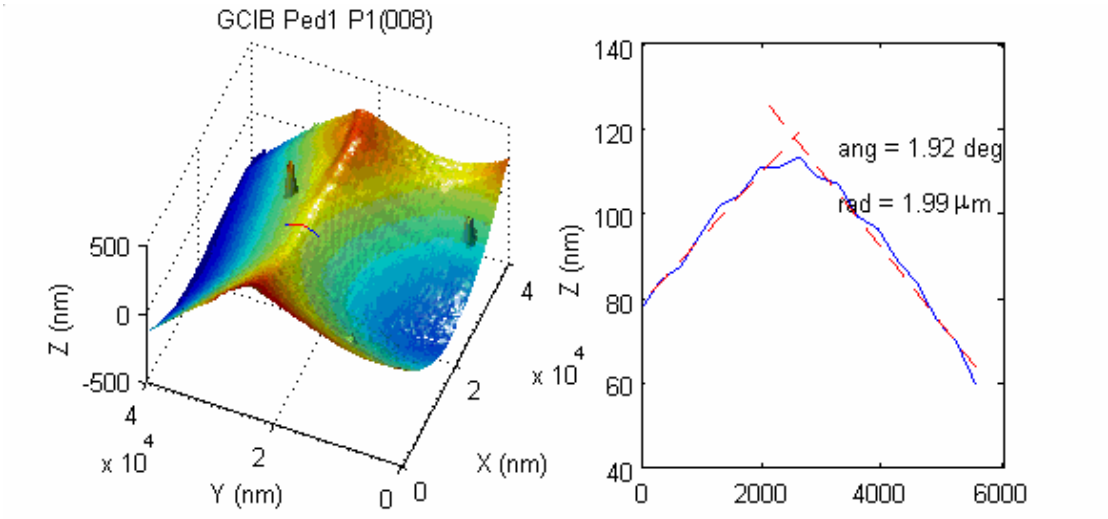

Figure 48: AFM image of grain boundary shown in red box in previous SEM image on the right.

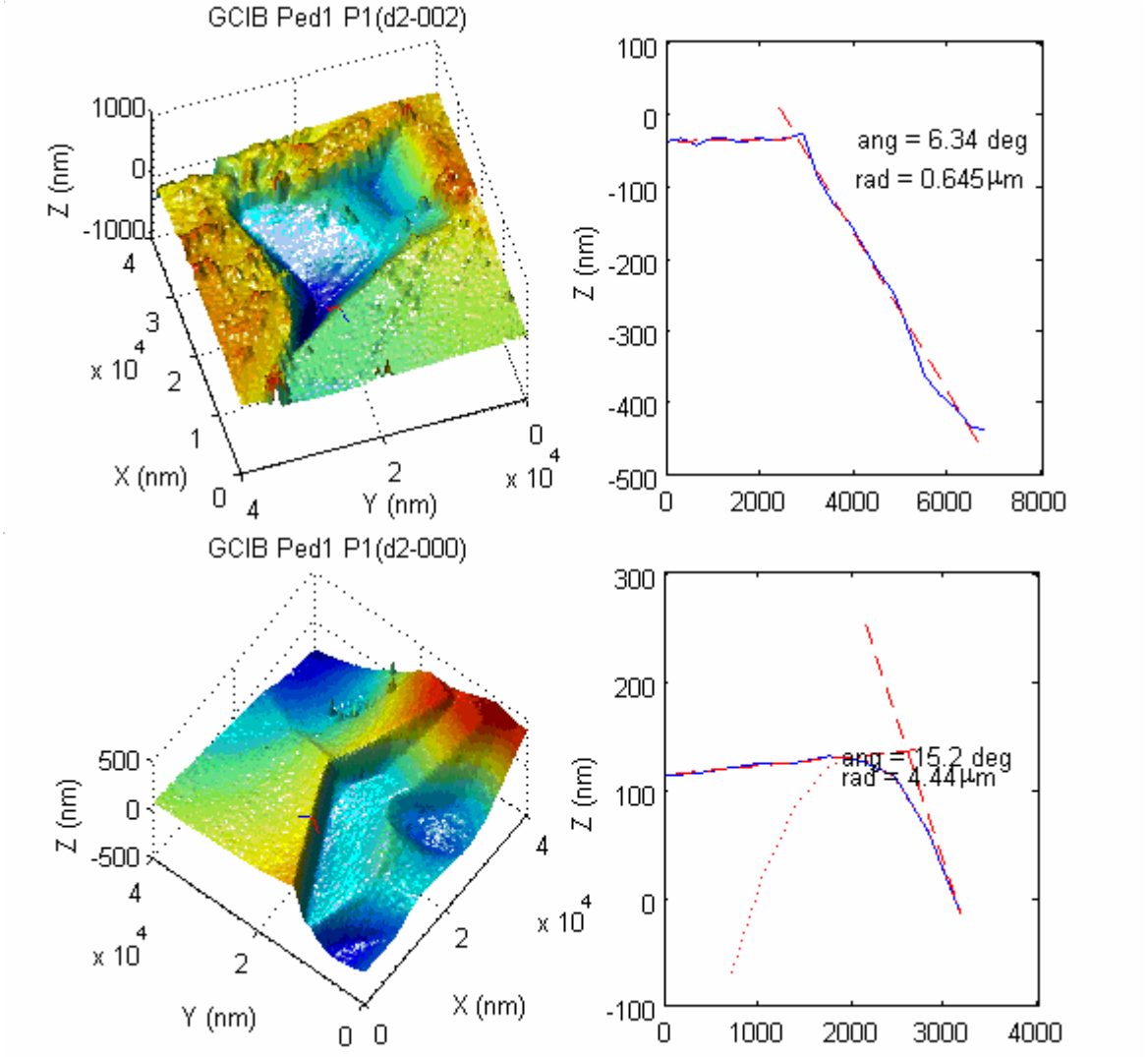

Figure 49: More AFM images of niobium after NF_3 + 0_2 GCIB processing

3.3. Results Summary and Conclusions.

A table (Table 3) that summarizes the measurements and graphical summaries of the AFM results are presented here. The profiler results (Table 1) have also been reproduced here for ease of comparison. Several graphs have been made of the

same data, since I couldn't think of a way to graph all of the results in an intuitive way in 2 or 3 dimensions. I have tried to be consistent with my labels: diamonds represent RRR 300, asterisks (*) represent RRR 500, red represents BCP 1:1:2, magenta represents BCP 1:1:1, and blue represents FNS 1:1:1. Less consistently, dots represent oxypolished samples and circles were used for the pedestals of the gas cluster bombarded sample (with red being used for the unprocessed pedestal, which is RRR 300 BCP 1:1:2). These results are shown in Figure 54 - Figure 58. A table of all results may be found in appendix 4.

Table 2: Reproduction of Table 1: Profiler results for ease of comparison.

Sample	RMS Rough. (μm)	Peak-Peak Rough. (μm)	Total length profiled (μm)
BCP 1:1:2	1.41	6.26	6,500
BCP 1:1:1	1.07	4.84	8,500
FNS 1:1:1	3.49	11.7	7,500
EP	0.12	0.66	8,500
500 RRR FNS 1:1:1	2.45	11.2	10,000
500 RRR BCP 1:1:2	1.03	5.57	20,000
500 RRR FNS 1:1:2	4.61	22.8	9,000

Table 3: Summary of AFM measurements

Sample	Mean Angle (°)	Std Dev Angle	Mean Radius of Curv. (μm)	Std Dev Radius	# meas. taken
BCP 1:1:2	12.0	4.1	0.43	0.51	3
BCP 1:1:1	10.2	3.4	2.79	2.86	9
FNS 1:1:1	52.8	23.5	0.40	0.39	11
500RRR FNS1:1:1	61.7	22.2	0.59	0.57	4
500RRR FNS1:1:2	44.8	17.6	0.38	0.21	5
500RRR BCP1:1:2	8.1	3.9	0.97	0.53	10
BCP1:1:1 oxypolished	16.9	9.8	2.27	4.16	13
BCP1:1:2 oxypolished	6.6	1.5	4.93	5.80	6
RRR500 BCP1:1:1	8.5	3.7	2.39	2.95	9
GCIB unproc	12.8	5.3	2.71	3.50	11
GCIB Ar	12.0	6.4	2.88	2.61	13
GCIB Ar+H2	11.8	4.7	5.06	5.02	6
GCIB Ar+CH4	5.6	2.4	1.43	0.96	7
GCIB NF3+02	4.8	4.6	3.39	3.19	8

The spreads in the data are considerable. However, certain conclusions are nonetheless suggested.

1. The first thing that jumps out from Figure 56 is that the high-β region (up and to the left—high angle and small radius) is pretty well dominated by the FNS samples (blue and black), and that these points, for the most part, are contained to this region. One area in which my data are lacking is the step height, which in addition to step shape, plays a roll in determining the β. So, bearing this in mind as a possible flaw, I would conclude that the FNS surfaces are going to make poorer RF surfaces as far as Q-slope goes. This is also quite apparent from Figure 54, though not from Figure 55. (It is worthy of note that this may not be supported, but it certainly not contradicted, by the results of profilometry (Table 1), which also hinted that the FNS surface may be rougher than the BCP surface (at least on a large scale).

2. The next most apparent thing that one sees (Figure 54, Figure 58) is that the GCIB treatment with NF_3O_2 (cyan circles) certainly tends toward the low-β region (down and to the right—low angles and high radii). One of the other treatments ($Ar+H_2$, black circles) may also have had an effect, but it is less clear. It makes some sense that ion bombardment with fluorine ions and oxygen may etch niobium effectively, since this is similar to the process that happens in chemical etching (oxidation of the niobium, then the oxide being removed through interactions with the fluoride ions). Another note to make about the GCIB samples is that they did, by and large, seem to be etched nonuniformly, ie, with some areas smoothed out quite nicely and some areas seemingly untouched.

3. A third observation which is suggested (but by no means demanded) by the data is that the higher purity RRR 500 niobium etched in BCP may be smoother

than the lower purity niobium. This is most apparent as a slight shift in Figure 54 and Figure 55, though it might be seen in Figure 58. Though these small shifts are not very strong evidence at with such small numbers of measurements taken, the fact that they are supported by the profiler data (Table 1 indicates that the RRR 500 BCP 1:1:2 is smoother than the 300 RRR) and the fact that this is more likely to affect actual cavities in the foreseeable future than, say, GCIB processing, makes further investigations worthwhile (in my opinion). A caveat would be that the grain size on the RRR 500 sample does seem to be slightly smaller than on the RRR 300, and so the step size may also be smaller as a result of that instead of having anything to do with purity, which may weaken a conclusion drawn from the profiler data. Interestingly, in as yet unpublished results[13] from this group suggest that Q-slope is somewhat milder in cavities made from this higher purity RRR 500 niobium (Figure 50).

[13] Thank you to Gregory Eremeev for showing this data to me, and for its use here.

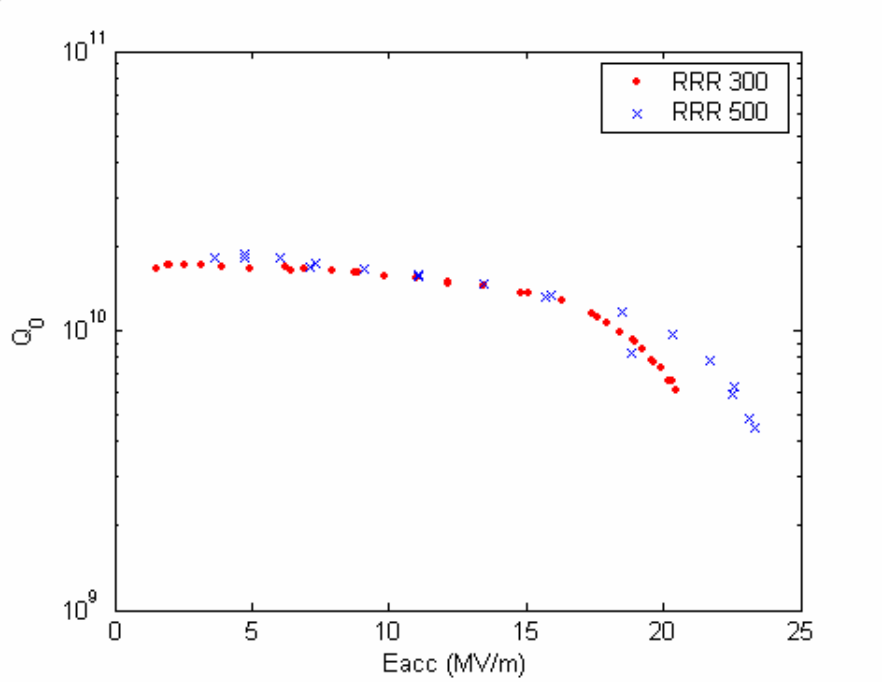

Figure 50: Comparison of Q-slope for 300RRR and 500RRR cavities (yet unpublished) [13]

4. It is also worth saying something about oxypolishing. In my first looks at the graphs and Table 3, I thought that there was evidence that the process helped smooth the grain boundaries some. However, I then noticed that the oxipolishing looks like it helped for BCP 1:1:2, and had the opposite effect (sharpened he boundaries!) for BCP 1:1:1 (which was essentially indistinguishable from BCP 1:1:2 under the SEM and AFM). I believe that this is just an anomaly of the sort that happens when ones sample size is too small. This, coupled with the strange cratering of the surface (Figure 37) leads me to conclude that oxypolishing does not, in fact help polish the surface better than BCP alone to a worthwhile extent.

5. A note on calculating magnetic field enhancement factors (β). I had originally hoped to use the data I took to calculate β's and perhaps estimate a distribution of field enhancement factors *n(β)* for at least some of the samples, to see if it

would be consistent with the distribution required by Knobloch [1] to explain Q-slope. I unfortunately never got around to doing this. In that paper, β were calculated for a certain geometry of grain boundary step: a step about 10μm tall, with a radius of curvature of 1μm and for various angles (Figure 52). My measurements are different from this geometry in a few important ways, namely the step height. I did not measure step heights systematically, but they were generally of order 0.5 - 2.0 μm (as seen from profiler data). This could be significant because it is smaller than the step height of 10 μm that he used in his calculations, meaning actual β may be smaller than he had used in his calculations of Q-slope. However, I did find a number of grain boundaries with radii of curvature significantly smaller than 1 μm (which he used in his simulations), which may offset this. It is worthy of note that only very few grain boundaries need to become normal conducting (i.e., have a high β) in order to explain the Q-slope. As shown in Figure 51 (the result of a calculation I did which was inspired and facilitated by [1]), only about the highest 1-3% of β ever become normal-conducting before the cavity breaks down. Because of this, I would say that my findings are not inconsistent with the distribution required in [1].

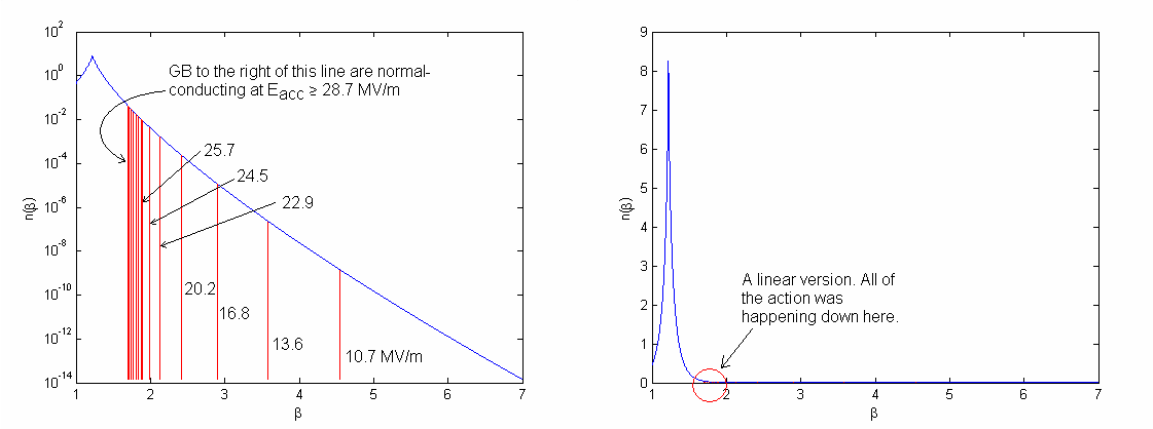

Figure 51: Very few (< 3%) of grain boundaries need to become normal-conducting to cause Q-slope or a quench. The distribution has been normalized so that its area is 1. (the vertical axis ranges from 10^{-14} to 10^{2}, and the horizontal (β) axis ranges from 1 to 7 on the left graph)

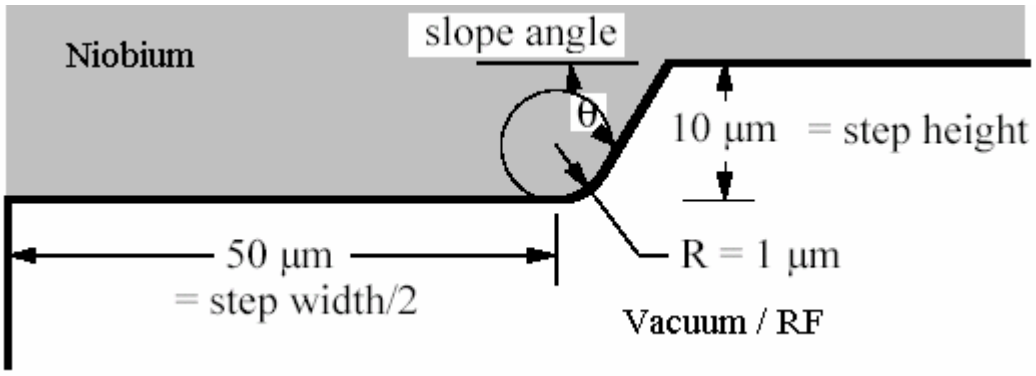

Figure 52: Geometry used by Knobloch et al [1] in their calculaion of b. Metal is above, vacuum (inside of RF cavity) is below.

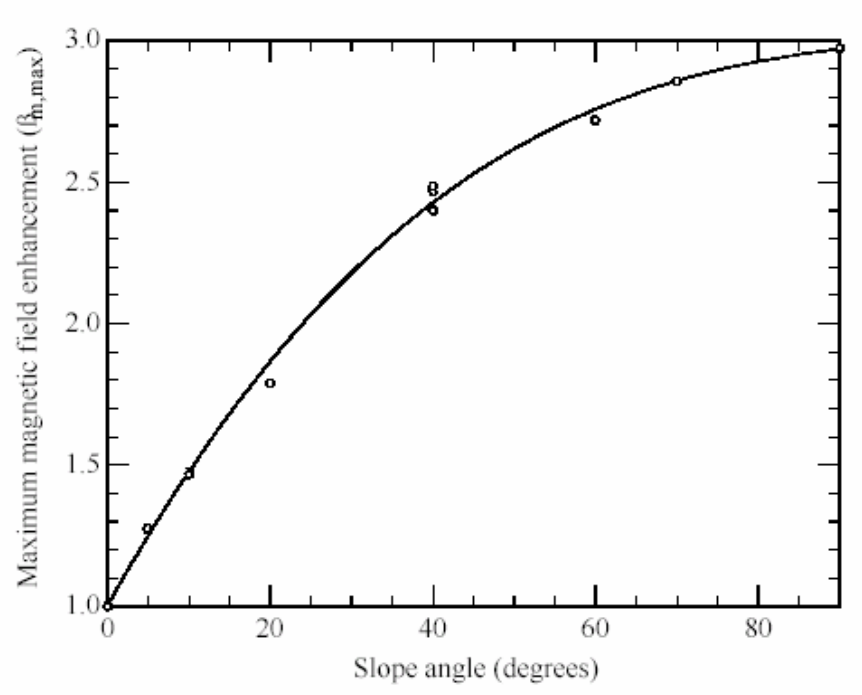

Figure 53: Calculations of beta for various GB shapes, from [1].

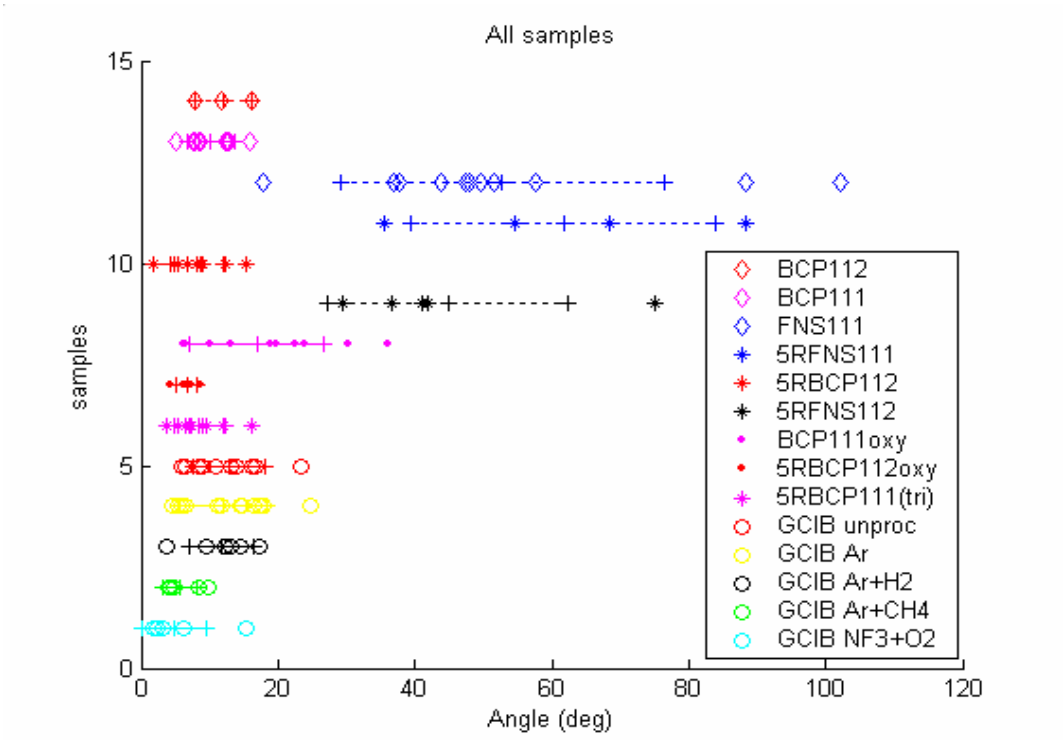

Figure 54: Summary of angles measured for various samples. Horizontal lines represent the region within one standard deviation of the mean for each sample.

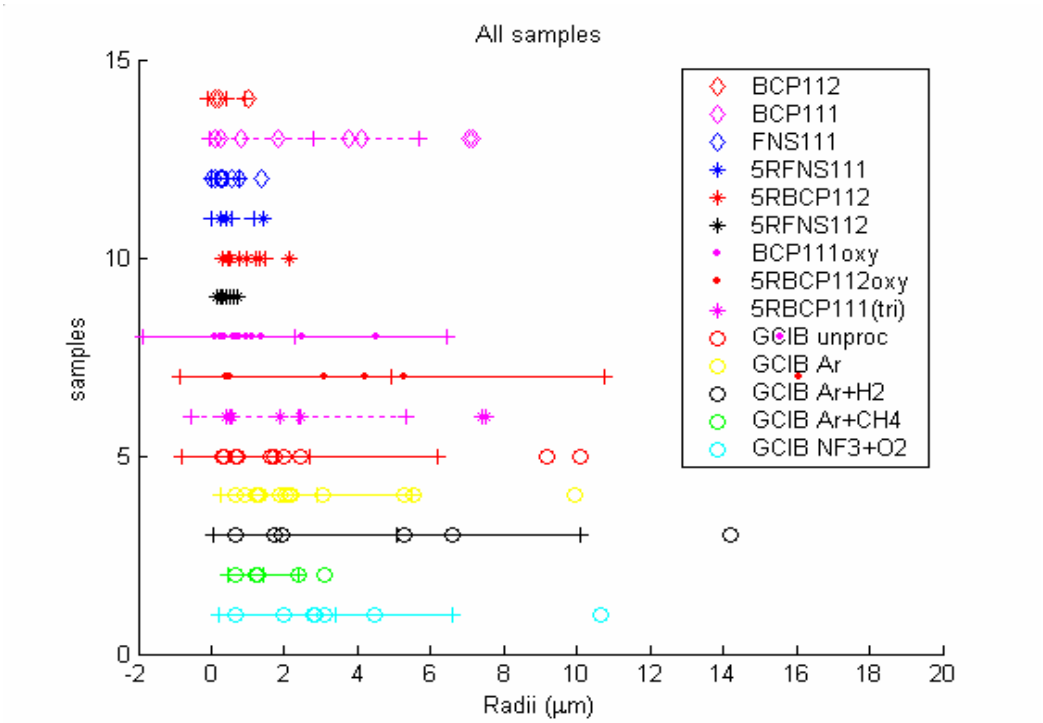

Figure 55: Summary of radii measured for various samples. Horizontal lines represent the region within one standard deviation of the mean for each sample. Please note the two data points inside the legend.

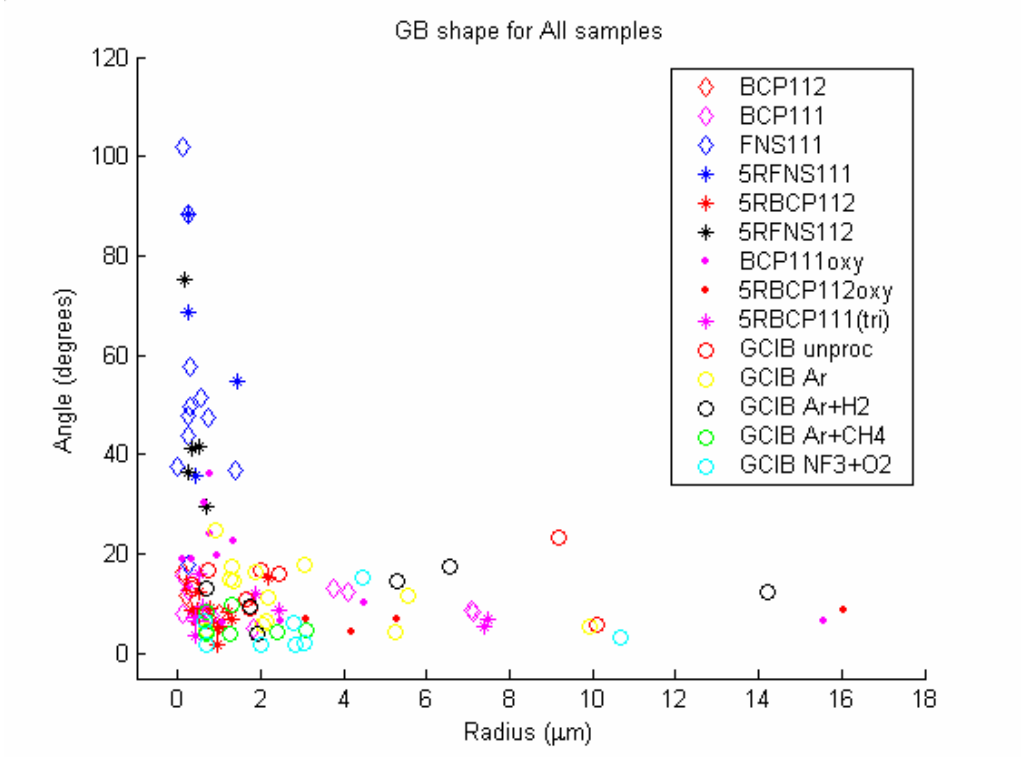

Figure 56: Graphical summary of results.

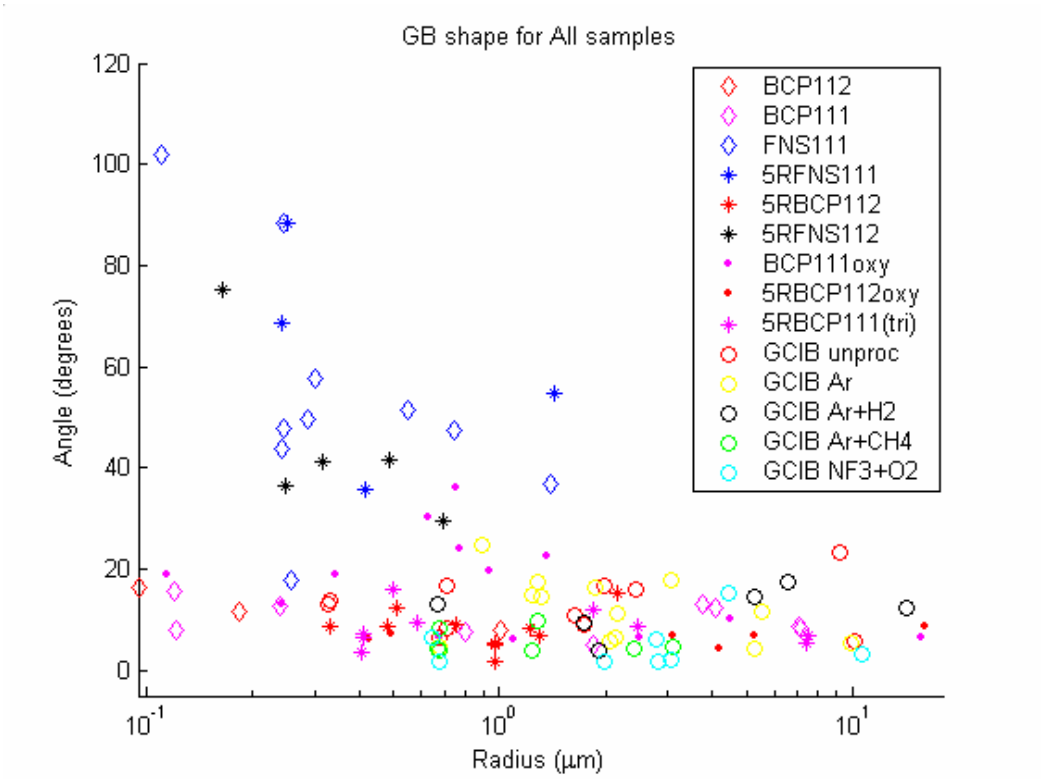

Figure 57: Same data as Figure 56 but with the radius plotted on a logarithmic scale to try to make individual points more visible.

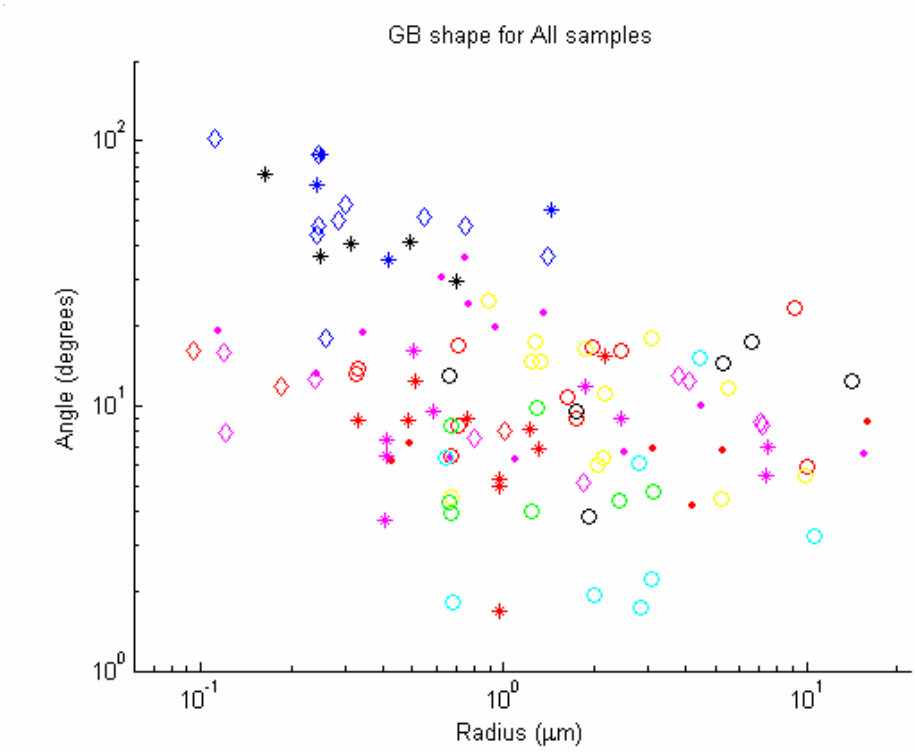

Figure 58: Same data as Figure 56, but with both axes on logarithmic scales in an attempt to make the data points more visible. In an effort to maximize visibility, the legend was removed; It is the same as Figure 56 and Figure 57.

4. Notes for Future Work

In order to better pin down these results, it would be very helpful to be able to identify several grain boundaries with the SEM, measure their characteristics with the AFM, then subject the sample to processing and look at the same grain boundaries again (this obviously does not apply to seeing a difference between RRR 300 and 500 samples). I had a great deal of trouble doing this with my samples—finding a specific 50 μm grain on a sample with a few cm^2 of area is very much akin to finding the proverbial needle in the haystack (this is further complicated by the fact that things look quite different under the SEM and under the optical microscope that one uses to line up the AFM (Figure 59). At one point I tried making a scratch on one of the samples and using that as a reference point, but the scratch was just too big (and it was only about 5 mm long). I decided that I would just try to take enough measurements that some statistical results could be attained, but I don't think that this worked out very well. The differences between the various samples results were generally not dramatic enough to be obvious with the amount of data I was able to take, and it just takes a long time to get sizeable amounts of AFM data. And no matter how much you do take, some people will still (and justifiably so) be skeptical of any result. Greg Werner has for several years used quarter-sized niobium samples with several ~$1mm^2$ pedestals machined into them. We used one of these samples for the GCIB investigation, and it was much easier to correlate SEM and AFM images. So, if anyone is to try this again, I would suggest using a sample with roughly square-millimeter sized

pedestals. It probably won't be possible to use the profiler on them, but you won't need it—the AFM will give you the answer. Another note is that, while large-scale (>15 μm, say) images are nice to look at and possibly important for gaining context (and correlating AFM and SEM images), smaller scale (<5 μm, say) are much easier to take (they will have a smaller vertical range, and the AFM really doesn't like large vertical ranges) and will provide a better spatial resolution for measuring the radius of curvature.

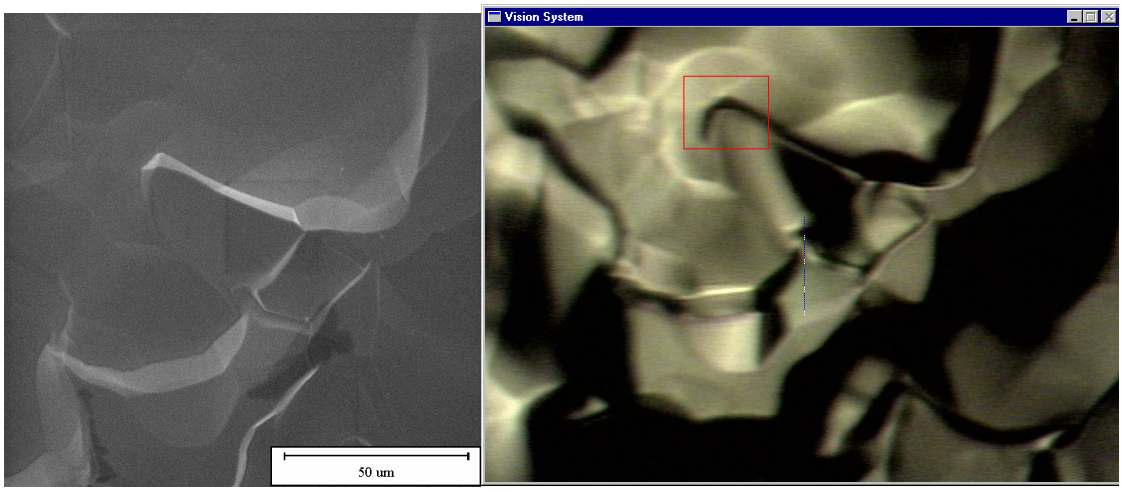

Figure 59: Comparison of the same region under the SEM (left) and he AFM's optical microscope (right). The scale bar is 50 μm.

It would also be very nice to somehow calculate the field enhancement factors of the shapes I have measured. Jens Knobloch[1] had calculated field enhancement factors for certain step shapes with the finite element code *SUPERLANS*. The shapes he looked at, however, were not representative of those that I have found. I think it would be a fairly quick matter to use his method to find β for some

of my grain boundary shapes, and see if they are consistent with his calculation of the distribution required to produce a Q-slope.

Finally, I wish to restress that taking another look at the difference between RRR 500 and RRR 300 samples etched in BCP 1:1:2 may be very worthwhile, since my results suggested (but only suggested) that the higher purity niobium may have a positive impact on the RF surface. It may be valuable to know more about this.

5. Acknowledgements

I would like to thank Hasan Padamsee for instruction, guidance, and the occasional kick in the pants as motivation. I would also like to thank Greg Werner for guidance, helpful discussions, and the occasional kick in the pants or dry criticism as motivation. I would like to thank Rong Li Geng and the fellows at Argonne National Lab and Epion Corp for providing me with some samples, and to Curtis Crawford for getting started with anodization. Thank you to the SRF lab crew (Phil Barnes, Rick Roy, Ethan Miller) for plentiful technical advice and for preventing me from electrocuting, drilling holes in or welding myself, to the chem room crew (Holly Conklin and Terry Gruber) for so far preventing my bones from being dissolved by HF, and to the office girls for various assistance, laughs and coffee. I would also like to acknowledge the work of Jens Knobloch, Rong Li Geng, and Hasan Padamsee, all of whose shoulders I have certainly stood on though I still don't think I can see as far as they have.

6. Appendices

Appendix 1: Current measurements for anodization

I recorded the anodization currents for several, but not all, of my procedures. Measurements labeled as “time = 0s” may be quite inaccurate, as the current changes quite wildly for the first few seconds. Other current measurements should be good a few per cent. Voltage measurements may vary a bit more (perhaps 5-10%) as my voltage source was homemade and fluctuated a bit. Time measurements are good to a second or two. Samples had a few square cm submerged in the anodizing solution.

V_start = 0v	V_end = 30V
Time (min)	**Current (mA)**
0	23
0.25	6
0.5	4.6
0.75	4.0
1.25	1.64
1.75	0.76
2.25	0.67
2.75	0.45
3.25	0.42
3.75	0.39
4	0.37

V_s = 30V	V_e = 60V
Time (min)	**Current (mA)**
0	50
0.5	33
1.0	12
1.5	5
2.0	2.2
2.5	1.67
3	1.3
3.5	1.22
4	1.11
4.5	1.12
5	0.80
5.5	0.75
6	0.69

V_s = 0V	V_e = 60V
Time (min)	**Current (mA)**
0	80
0.5	19
1.0	5
1.5	2.5
2.0	1.6
2.5	1.5
3	1.11
3.5	1.04
4	0.99
4.5	1.92

V_s = 0V	V_e = 60V
Time (min)	**Current (mA)**
0.0	70
0.25	32
0.5	17
0.75	7
1.0	4.6
1.5	2.2
2.0	1.85
2.5	1.35
3.0	1.17
3.5	0.93
4.0	0.87
4.5	0.84

V_s = 0V	V_e = 70V
Time (min)	**Current (mA)**
0	88
0.25	42
0.5	20
0.75	7.3
1.0	3.4
1.5	2.3
2.0	2.06
3.0	1.5
3.5	1.37
4.0	1.26
4.5	1.04
5.0	0.94

V_s = 70V	V_e = 80V
Time (min)	**Current (mA)**
0.0	4.5
0.25	4.0
0.5	3.75
0.75	3.56
1.25	3.05
2.0	1.99
3.0	1.45
4.0	1.09
5.0	0.89

V_s = 80V	V_e = 90V
Time (min)	**Current (mA)**
0.25	6.48
0.5	5.94
0.75	4.48
1.0	3.78
1.5	3.3
1.75	2.52
2.0	2.34
2.5	1.81
3.0	1.69
3.5	1.27
4.0	1.17
4.5	0.93

V_s = 90V	V_e = 100V
Time (min:sec)	**Current (mA)**
0:10	6.6
0:20	6.2
0:30	5.78
0:40	5.05
0:50	4.68
1:00	4.42
1:30	2.66
2:00	2.13
2:30	1.84
3:00	1.51
3:30	1.36
4:00	1.13
5:00	1.01
7:00	0.78

V_s = 100V	V_e = 110V
Time (min)	**Current (mA)**
0.25	5.3
0.5	4.0
0.75	3.73
1.0	3.22
1.5	2.42
2.0	2.04
2.5	1.46
3.0	1.4
4.0	1.16
5.0	0.91
6.0	0.85

V_s = 0V	V_e = 60V
Time (min:sec)	**Current (mA)**
0:00	70
0:10	43
0:20	30
0:30	15
0:40	7
0:50	5
1:00	2.8
1:30	2.2
2:00	1.43
2:30	1.24
3:00	1.12
3:30	0.94
4:00	0.82
4:30	0.73
5:00	0.70

V_s = 60V	V_e = 110V
Time (min)	**Current (mA)**
0:10	41
0:20	22
0:30	9
0:40	5.5
0:50	4.4
1:00	3.38
1:30	2.35
2:00	1.56
2:30	1.42
3:00	1.29
3:30	1.05
4:00	0.96
4:30	0.93
5:00	0.82

These results are summarized on Figure 60. Some of the variation may be explained by the different voltages being used (the solid lines are all 10V steps, and fall below almost all of the others) and by differences in surface area of the samples (and the niobium wires holding them) which was submerged (I tried to keep this constant, but there were some differences. Plus, two different samples of different surface areas were used.

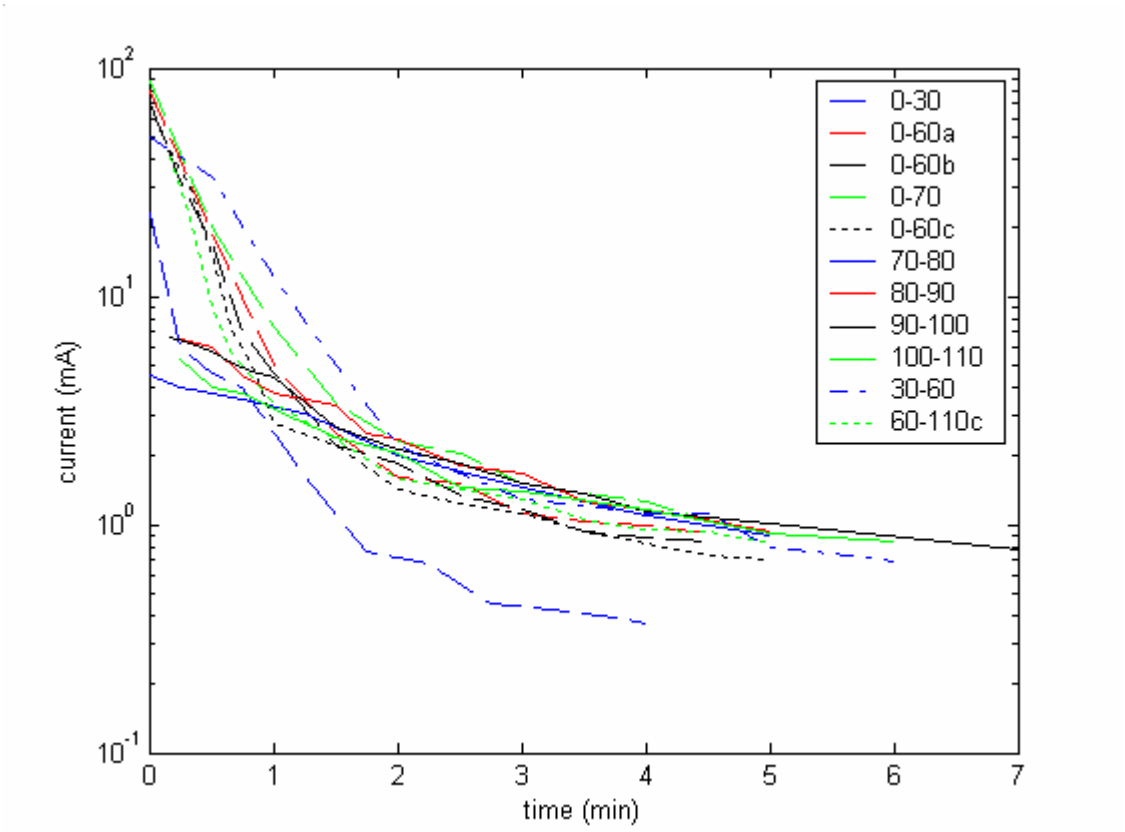

Figure 60: Anodization currents on a semilog plot.

I tried to integrate these curves to plot total charge (which should be proportional to oxide thickness) versus voltage to observe the linearity of the 20A / Volt discussed earlier, but with ambiguous results (probably due to the intricacies

involved in numerically integrating sparse and somewhat inaccurate data, and the variation in amount of wire tongs submerged, etc.). The black asterisks (one series of runs) could conceivably be points on a line through the origin, but the red circles and blue dots do not seem to be.

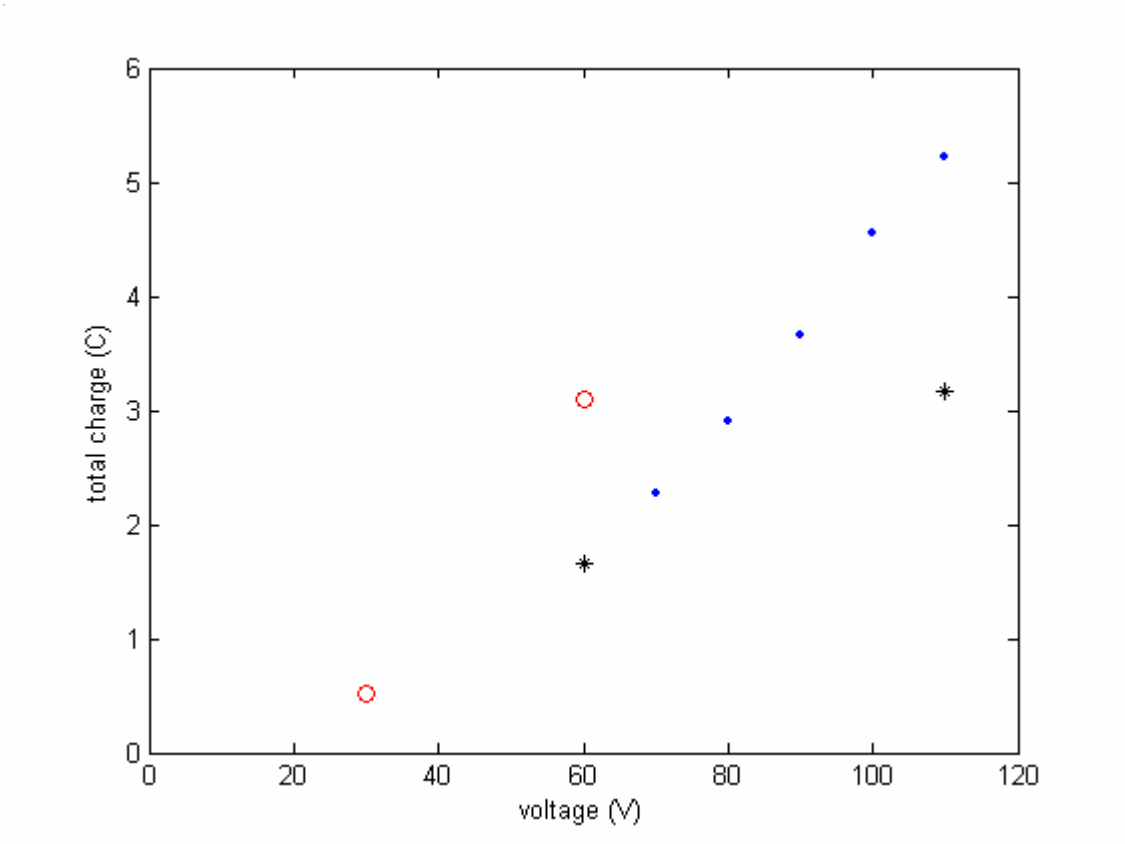

Figure 61: Total charge (hence total oxide grown) versus voltage, from integrating Figure 60.

Appendix 2: Instructions for making a 3D SEM image with GIMP

Take one image with the SEM. Tilt the sample by 7-10 degrees, find the same field of view, and take another image. Import the first (untilted) image into the GIMP (GNU Image Manipulation Program) and put it on one layer. Import the tilted image onto a second layer. You may have to rotate these images by 90 degrees to make the tilt axis appropriate to right-eye / left-eye difference. E.g., the tilt axis on our SEM is horizontal in the unrotated images, such that the tilted image is what would be seen by an eyeball *above* the eyeball which sees the untilted image, rather than an eyeball to the *right* of the untilted. As such, I rotate the images by 90 degrees clockwise. There should be a "subtract one layer from another" option, allowing you to see the difference between the two images. You should select this and move the tilted layer around to minimize the difference between the images. If you have to choose, you should make the frontmost features line up best. You can also stretch the tilted image to correct for the foreshortening which results from being tilted, which will make the image easier to look at. Now, as cellophane 3-D glasses have the red cellophane in the left lens and the blue in the right, you will want to make sure that you get the colors on the images right. Select the image layer corresponding to the left eye (in my case, the tilted image), change to RGB mode, and remove the red. Select the other image and remove the green and blue. Now flatten the image to one layer, and you should have a 3D, red-blue glasses image[14].

[14] Thank you to Peter Lee, at the Applied Superconductivty Center, Univ. of Wisconsin-Madison, for getting me started with this procedure.

Appendix 3: Profiler measurements.

Sample	RMS height (μm)	P-P height (μm)	Profile Length (μm)
RRR 300 BCP 112	1.60	7.29	2000
	1.40	6.89	2000
	1.68	5.47	500
	1.50	6.22	2000
	1.49	7.15	2000
	1.54	6.47	2000
	1.27	6.23	2000
	1.07	4.39	500
RRR 300 BCP 111	1.31	5.14	500
	1.28	5.51	2000
	0.92	5.10	1000
	0.68	4.17	1000
	1.06	5.46	1000
	0.97	3.80	1000
	1.02	4.65	1000
	1.24	4.85	1000
300 RRR FNS 111	1.95	8.16	500
	4.55	19.4	2000
	2.66	9.55	2000
	1.95	7.62	500
	2.34	7.44	500
	4.32	18.0	2000
300 RRR EP	0.11	0.58	2000
	0.16	0.85	2000
	0.10	0.61	2000
	0.13	0.58	500
	0.12	0.68	2000

Sample	RMS height (μm)	P-P height (μm)	Profile Length (μm)
500 RRR FNS 111	2.70	10.1	2000
	2.91	12.6	2000
	1.68	8.66	2000
	1.97	8.53	2000
	2.97	15.1	2000
500 RRR BCP 112	1.04	5.76	2000
	1.05	4.31	2000
	0.94	4.62	2000
	0.95	4.61	2000
	0.80	3.97	2000
	1.08	5.85	2000
	1.23	5.99	2000
	1.22	7.03	2000
	1.24	8.72	2000
	0.88	4.81	2000
500 RRR FNS 112	7.32	29.6	1000
	4.41	25.1	2000
	4.57	20.5	2000
	4.03	17.3	2000
	4.74	21.4	2000

Appendix 4: AFM measurements

Angle measurements are typically good to about 2-3 degrees. Radii, I have somewhat less confidence in; but they should be good to 5-10%, except that some are upper bounds.

Sample	Angle (rad)	Radius (nm)	Sample	Angle (rad)	Radius (nm)
RRR 300 BCP 1:1:2	0.283	94.8	RRR 500 BCP 1:1:2	0.092	974
	0.140	1013		0155	330
	0.205	184	RRR 300 BCP111oxy	0.230	243
RRR 300 BCP 1:1:1	0.150	7071		0.174	4498
	0.089	1843		0.110	1098
	0.221	239		0.346	941
	0.276	120		0.328	344
	0.133	798		0.332	114
	0.226	3755		0.632	752
	0.216	4102		0.419	773
	0.146	7137		0.112	673
	0.139	121		0.114	15571
RRR 300 FNS 1:1:1	0.312	258		0.116	2500
	0.830	745		0.529	629
	1.781	111		0.391	1364
	1.005	302	RRR 500 BCP112oxy	0.073	4189
	0.899	549		0.120	3112
	0.835	244		0.107	428
	0.867	285		0.119	5298
	0.644	1391		0.152	16067
	0.658	0		0.126	493
	0.658	244	500 RRR BCP1:1:1	0.129	412
	1.542	241		0.064	408

Sample	Angle (rad)	Radius (nm)	Sample	Angle (rad)	Radius (nm)
RRR 500 FNS 1:1:2	0.729	0.729		0.112	412
	0.516	0.516		0.155	2458
	0.717	0.717		0.095	7385
	0.639	0.639		0.165	583
	1.311	1.311		0.280	502
RRR 500 BCP 1:1:2	0.143	1224		0.121	7492
	0.029	967		0.207	1853
	0.215	513	GCIB unprc	0.148	707
	0.087	970		0.157	1744
	0.270	2156		0.281	2444
	0.153	483		0.103	10104
	0.120	1304		0.113	674
	0.156	758		0.189	1632
GCIB unprc	0.243	333	GCIB Ar+H2	0.302	6567
	0.291	1979		0.067	1909
	0.407	9162		0.252	5298
	0.294	710	GCIB Ar+CH4	0.070	1238
	0.231	328		0.171	1286
GCIB Ar	0.078	5252		0.146	673
	0.079	673		0.076	667
	0.258	1236		0.069	674
	0.104	2044		0.082	3102
	0.433	898		0.076	2404
	0.314	3062	GCIB NF3+O2	0.032	680
	0.204	5541		0.033	1993
	0.095	9941		0.266	4444
	0.256	1321		0.039	3071
	0.303	1280		0.030	2823
	0.286	1857		0.111	645
	0.111	2121		0.057	10657
	0.194	2162		0.107	2797
GCIB Ar+H2	0.217	14203			
	0.227	666			
	0.165	1741			